JONATHAN GAREAU

69717

A Numerical Study of Submesoscale Processes in the Coastal Circulation of Madeira

UAlg FCT
UNIVERSIDADE DO ALGARVE
FACULDADE DE CIÊNCIAS E TECNOLOGIA

2022

University of Algarve
Faculty of Science and Technology
Master of Science – Marine and Coastal Systems

Dissertation

A Numerical Study of Submesoscale Processes in the Coastal Circulation of Madeira

Jonathan Gareau, 69717

Supervisors:

Rui Caldeira (ARDITI-Agencia Regional para o Desenvolvimento da Investigação, Tecnologia e Inovação, OOM-Oceanic Observatory of Madeira)

João Janeiro (University of Algarve, CIMA-Centre for Marine and Environmental Research)

Flávio Martins (University of Algarve, CIMA-Centre for Marine and Environmental Research)

2022

Declaration of Authorship of Work

A Numerical Study of Submesoscale Processes in the Coastal Circulation of Madeira

I, Jonathan Gareau, declare I am the author of this work, which is original and unpublished. The sources consulted have been duly cited in the text and included in the list of references.

_____

Jonathan Gareau

Abstract

Submesoscale processes are defined geometrically by a lower length scale than the first baroclinic radius of deformation and dynamically by a Rossby number (*Ro*) of O(1), thus virtually unaffected by planetary forces. They have been widely studied in various environments using in-situ measurements, remote sensing, and numerical modelling. However, due to their unpredictable nature and relatively short spatial and temporal scales, identifying submesoscale patterns is a difficult task. Therefore, abundant ongoing research is continuously seeking new insight on their irregular behavior in the ocean. Recent observations of submesocale structures have shown their efficiency in transporting particles horizontally and vertically in both the open ocean and coastal waters. Oceanographic studies concerning the deep-sea island of Madeira have mainly focused on mesoscale processes but have yet to describe features found at the submesoscale. Based on the recent discovery of a coastal current over Madeira's insular shelf, this study attempts to assess the role of submesoscale processes on the island's coastal circulation and the main physical forcings responsible for their generation. A coupled ocean-atmosphere model (COAWST) was used to simulate oceanic outputs within 1-km resolution grids, from which Eulerian properties of the flow field were calculated to detect submesoscale activity in the area. In addition, 4 simulations were run according to different forcing scenarios: (A) all forcings (wind, tides, geostrophic); (B) wind forcing; (C) tidal forcing; (D) geostrophic far-field forcing. Results show that submesoscale activity was generally concentrated near the coast and mostly attributed to wind and geostrophic forcings. Eddies with *Ro* larger than 1 were found in Madeira's wake and/or on the fringes of mesoscale eddies interacting with the island's shallow bathymetry, which is in line with the literature. These small-scale eddies were the dominant feature within the coastal circulation, suggesting their important contribution to the material transport along the shelf.

Keywords: Submesoscale, Eddies, Coastal circulation, Madeira, Deep-sea islands, Ocean modelling, COAWST.

Sumário

Os processos de submesoscala são definidos geometricamente por uma escala de comprimento inferior ao primeiro raio de deformação baroclínico e dinamicamente por um número Rossby (*Ro*) de O(1), praticamente não afectado por forças planetárias. Estes têm sido amplamente estudados em vários ambientes utilizando medições in-situ, detecção remota, e modelação numérica. No entanto, devido à sua natureza imprevisível e escalas espaciais e temporais relativamente curtas, a identificação de padrões de submesoescala é uma tarefa difícil. Por conseguinte, existe muita investigação em curso à procura de uma melhor compreensão do seu comportamento irregular no oceano. Observações recentes de estruturas de submesoescala demonstraram a sua eficiência no transporte horizontal e vertical de partículas tanto no oceano aberto como nas águas costeiras. Focando nas águas profundas da ilha da Madeira, vários estudos oceanográficos centraram-se principalmente nos processos de mesoscala, mas ainda não descreveram as características encontradas na submesoscala. Com base na recente descoberta de uma corrente costeira sobre a plataforma insular da Madeira, este estudo tenta avaliar o papel dos processos de submesoescala na circulação costeira da ilha e os principais forçamentos físicos responsáveis pela sua geração. Foi utilizado um modelo numérico acoplando as interações oceano-atmosfera (COAWST) para simular saídas oceânicas dentro de grelhas de 1 km de resolução, a partir das quais foram calculadas as propriedades eulerianas do campo de fluxo para detectar a actividade de submesoescala na área. Além disso, foram efectuadas 4 simulações de acordo com diferentes cenários forçadores: (A) todos os forçamentos (vento, marés, geostróficos); (B) forçamento pelo vento; (C) forçamento pela maré; (D) forçamento pelo campo distante geostrófico. Os resultados mostram que a actividade de submesoescala foi geralmente concentrada perto da costa e atribuída principalmente aos forçamentos pelo vento e geostrófico. Foram encontrados eddies com *Ro* maior que 1 na esteira da Madeira e/ou nas franjas de eddies de mesoescala interagindo com a batimetria rasa da ilha, o que concorda com a literatura. Estes remoinhos de pequena escala foram a característica dominante na circulação costeira, sugerindo a sua importante contribuição para o transporte de material ao longo da plataforma continental.

Palavras-chave: Submesoescala, *Eddies*, Circulação costeira, Madeira, Ilhas de mar profundo, Modelação oceânica, COAWST.

Acknowledgments

I would first like to thank the staff at the OOM for assisting me through this difficult learning process. A special thanks to Cláudio Cardoso for taking the time to teach me the basics (and the not so basics) of Python and really helping me put this thesis together. I left my comfort zone with this type of work, and your patience and scientific input were greatly appreciated. Thank you to Jesus Reis and Alexandra Rosa for the valuable help in the handling of the various datasets explored over the course of this project and to Rui Vieira for sharing your programming knowledge and expertise.

To my partner Raphaelle, I am so grateful for your daily attention and advice. I can always count on you, no matter the situation. Thank you to my friends in Faro, Gio, Azzu, Pol, for all the moral support from day one. And to my friends in Madeira, Alexandra, Gonçalo, Jesus, Eva, Rodrigo, and Luís Paulo, you have made my experience in this special island so much fun, thank you for all the nice moments. I will forever have "A Festa da Cebola" in my heart.

I would also like to mention the Maurice Group for their consistent entertainment throughout this journey. While I was in Portugal, their wise comments and unique humor made me feel closer to home. They even showed support and appreciation for when I was learning to speak Portuguese. Eu falo português!

Last but not least, I want to thank my supervisors Rui and João for guiding me through the many uncertainties and rerouting of this project and acknowledge the Portugal FCT (Fundação para a Ciência e Tecnologia) for the financial contribution in running the numerical simulations of this work.

Table of Contents

List of Figures

1. Introduction

Ocean processes and motions occur on a wide range of scales. Large scale dynamics, initiated by atmospheric winds, dictate the global ocean surface circulation. These large-scale motions then break into mesoscale processes O(10 km–100 km), which can be seen from space as they form eddies and meanders across oceans. These flows, where a significant amount of the ocean's kinetic energy reside, are mainly two-dimensional and dominated by horizontal advection. They most often remain in a state of hydrostatic and geostrophic balance from which energy is hardly dissipated by turbulence (Thomas *et al.*, 2008). Indeed, at these larger scales, the horizontal component of the flow usually exceeds the vertical component by 4-5 orders of magnitude (Mahadevan, 2006). This is due to the ocean geometry (small depth to length ratio) as well as the rotation of the earth and density stratification restraining vertical motion. Mesoscale eddies, which work similarly to atmospheric cyclones and anticyclones, are generally well understood and regularly observed with satellite altimeters (Stammer, 1997).

Recent studies, however, have shown that smaller scaled phenomena are very dynamic in the upper ocean and can drive much stronger vertical motions (1-2 orders of magnitude) than those associated with mesoscale flows (Capet *et al.*, 2008a). These small-scale oceanic processes are defined as submesoscale O(100 m–10 km), i.e., less than the first baroclinic deformation radius. Hydrographic features at this scale correspond to fronts, filaments and vortices, and are mainly generated through frontogenesis, baroclinic instabilities, and topographic wakes (McWilliams, 2016). Dynamically, submesoscale processes are characterized by O(1) Rossby (*Ro*) and Richardson (*Ri*) numbers, which differ from mesoscale processes ($Ro \ll 1$, $Ri \gg 1$) (Thomas *et al.*, 2008). In other words, currents at the submesoscale are less constrained by Coriolis force effects and instead governed by a higher degree of turbulence. The turbulent nature of submesoscale flows renders them irregular and without any clear spatial or temporal patterns.

Moreover, this submesoscale turbulence has important implications regarding the ocean's global circulation and energy budget. Baroclinic instabilities occurring at the submesoscale were first thought to be the transition between the non-dissipative mesoscale motions and the dissipative smaller-scale regime (McWilliams, 2003; Molemaker *et al.*, 2005; Müller *et al.*, 2005). In fact, submesoscale currents, despite being less energetic than mesoscale eddies, are associated with a loss of geostrophic and thermal wind balance, which translates into strong

ageostrophic effects in the mixed layer, thus generating greater vertical velocities (Mahadevan, 2016). This ageostrophic circulation can extract energy from the balanced state of mesoscales and transfer it to smaller, fully three-dimensional processes, typically ≤O(100 m), such as convection and internal waves (Thomas *et al.*, 2008). While these very fine scales may be responsible for energy dissipation in the ocean (Mahadevan, 2006), they cannot account for the diapycnal mixing required to achieve tracer balance and energy equilibrium in the ocean (Wunsch, 2004). Consequently, the ongoing research on submesoscale dynamics is crucial to further understand its role on horizontal and vertical distribution of properties in the ocean.

The transport of particles in coastal waters can be attributed to many different oceanic features (e.g., tides, internal waves, upwelling, eddies, turbulent mixing). Submesoscale currents, by creating various nearshore transport pathways, substantially contribute to coastal transport (Dauhajre *et al.*, 2019). The coastal processes near Madeira Island, a deep-sea island located in the northeast Atlantic Ocean, have been widely investigated, although limited to the study of oceanic features found at the mesoscale, particularly within its wake (Alves *et al.*, 2021; Caldeira *et al.*, 2002, 2014; Caldeira & Sangrà, 2012; Couvelard *et al.*, 2012). The 2014 oceanographic campaign POS466, using ADCP data, allowed the observation of a current shear at the edge of Madeira's insular shelf, where there was a considerable difference in the current speed and direction between nearshore and offshore waters (Reis *et al.*, in preparation). Lagrangian drifter trajectories, deployed on the island's southern margin, further confirmed an alongshore transport over the shelf, leading to the hypothesis of particle retention inshore and particle dispersion offshore (Reis *et al.*, in preparation). However, submesoscale motions and their role on the local transport in this coastal area have yet to be explored. Considering the established link between the meso- and submesoscales, mainly by driving the energy cascade in the ocean, and the contribution of nearshore submesoscale currents to the coastal transport, there is a clear motive to complement previous studies on the mesoscale regime and insular shelf circulation in Madeira with a better understanding of submesoscale processes.

Using numerical simulations from a coupled ocean-atmosphere model and Eulerian submesoscale-detecting parameters, this study will attempt to describe the role of submesoscale surface activity on the coastal circulation of Madeira. Additionally, by isolating atmospheric and oceanic forcings (wind, tides, geostrophic currents) into different simulations,

a parallel objective is to determine the influence of each of these physical forcings on the intensity, duration, and location of the submesoscale phenomena observable in the area.

Section 2 will provide a review of literature on the topic of submesoscale processes globally and in Madeira. The study area is introduced in section 3. A description of the data and methods used can be found in section 4. Sections 5 and 6 present the results and discussion, respectively.

2. Literature Review

2.1. Observations of Submesoscale Features

Submesoscale features in the ocean are difficult to observe due to their small horizontal scales, spontaneous appearance, and short lifetime (McWilliams, 2016). SST and ocean color satellites reveal ubiquitous submesoscale structures at the ocean's surface but cannot measure the underlying velocity fields. Furthermore, while the current generation of satellite altimeters, which have a resolution near the deformation scale (100 km), routinely observe currents at the mesoscale, they are still unable to resolve them at the submesoscale (Gula *et al.*, 2021).

Early evidence of such submesoscale features came from photographs of the Apollo Mission in the 1970s, which revealed spiral eddies with horizontal scales of 10-25 km (Munk *et al.*, 2000). More recently, numerical modelling, both from high-resolution simulations (Capet *et al.*, 2008a; Dong & McWilliams, 2007; Klein *et al.*, 2008; Mahadevan & Tandon, 2006) and parametrization studies (Boccaletti *et al.*, 2007; Calvert *et al.*, 2020; Fox-Kemper & Ferrari, 2008), has been the main tool to adequately reproduce and understand submesoscale dynamics. Zhong & Bracco (2013), with high-resolution model runs, were able to resolve vertically the first 150 meters of the water column, capturing large vertical velocities and dispersion of Lagrangian particles. However, with increasingly complex and high-resolution models, there remains a gap in modern observations as they are unable to generate measurements of currents and wind vectors and waves with a high enough spatial and temporal resolution to serve as model validation and parametrization tools. A recent satellite mission, SEASTAR (Gommenginger *et al.*, 2019), proposes to fill this observational gap by generating 1-km resolution images of total ocean surface current vectors, wind vectors and wave direction spectra based on Synthetic Aperture Radar interferometry. Likewise, the Ocean Surface Current multiscale Observation Mission (OSCOM, Du *et al.*, 2021) satellite launch is expected to make headway in observing submesoscale structures over the global ocean surface using Doppler Scatterometer technology at a horizontal resolution of 5–10 km and a 3-day global coverage. Furthermore, the Surface Water Ocean Topography mission (SWOT, Morrow *et al.*, 2019) aims to provide a global coverage of sea surface height at a resolution of 15-30 km, but the presence of other motions at similar spatial scales, such as internal waves, makes it challenging to reconstruct surface velocity fields at the submesoscale. Nevertheless,

recent studies (Rascle *et al.*, 2017, 2020) have obtained promising results of sea surface roughness using airborne (optical and radar) and satellite measurements at unprecedented accuracy, which allow the monitoring of submesoscale fronts.

Progress in the observation and quantitative characterization of submesoscale motions in the upper ocean come from dedicated multiplatform in-situ campaigns: AESOP (Johnson *et al.*, 2020); LATMIX (Shcherbina *et al.*, 2015); LATEX (Petrenko *et al.*, 2017); OSMOSIS (Buckingham *et al.*, 2016); ASIRI (Wijesekera *et al.*, 2016); M-AUE (Jaffe *et al.*, 2017); CARTHE's LASER and SPLASH (D'Asaro *et al.*, 2020); and CALYPSO (Mahadevan *et al.*, 2020). These observational programs usually require a combination of different field instruments (e.g., moorings, buoys, autonomous underwater vehicles) and ships, which are budget-heavy and logistically complicated to operate (Gula *et al.*, 2021). Moreover, surface drifters and High-Frequency (HF) radars were deemed practical and accurate tools for oceanographic research in coastal areas (Carlson *et al.*, 2010; Ohlmann *et al.*, 2005). Numerous studies have observed nearshore submesoscale features in the surface layer using data from surface drifters (Alpers et al., 2013; Esposito et al., 2021; Krayushkin et al., 2019; Nencioli et al., 2011; Ohlmann et al., 2017) or HF radars (Archer *et al.*, 2015; Chavanne *et al.*, 2010; Gildor *et al.*, 2009; Won *et al.*, 2019).

2.2. Submesoscale Circulation and Transport of Particles

2.2.1. Surface Processes and Transport

Submesoscale flows associated with coherent structures (e.g., fronts, filaments and vortices) are characterized by convergent surface currents, which concentrate buoyant material such as plankton, marine debris, and oil droplets (D'Asaro *et al.*, 2018). Through numerical simulations, Dauhajre *et al.*, (2017) demonstrated that these small-scall currents are ubiquitous on the Southern California shelf and are usually associated with fronts and filaments with strong cyclonic vorticity and daily time scales. The authors also discovered that surface material laterally advected within the shelf was preferentially trapped into the convergent lines of such frontal and filamentary structures and eventually driven into the ocean interior by the intense downwelling associated with convergence. Similar trapping patterns of surface particles were observed in submesoscale cyclonic eddies identified along the Eastern Australian Current from

in-situ and satellite data (Mantovanelli *et al.*, 2017; Schaeffer *et al.*, 2017). Furthermore, as shown by Gildor *et al.*, (2009) using high-resolution measurements of surface currents from HF radars and aerial photography, submesoscale barriers can halt horizontal mixing and trap passive scalars such as larvae or pollutants.

The control of Lagrangian trajectories by submesoscale currents has been commonly observed in both open-ocean (Berti *et al.*, 2011; Gula *et al.*, 2014; Lumpkin & Elipot, 2017) and coastal (Krayushkin et al., 2019; Ohlmann et al., 2017; Petrenko et al., 2017) regimes. Modeling studies (Romero *et al.*, 2013; Uchiyama *et al.*, 2014) have shown that submesoscale coherent structures on the shelf are more responsible for material dispersion than the mean currents and tides. These simulations also revealed that the nearshore lateral transport is highly anisotropic and generally aligned with the coastline, limiting cross-shelf dispersion. Concurringly, Nencioli *et al.*, (2011), using surface drifter measurements during the LATEX campaign, identified Lagrangian coherent structures that were flowing relatively parallel to the coast. In turn, water masses moving along the coastal margin encountering such submesoscale structures can slow down and see their residence time increase, which can induce high chl-a concentrations (Bolado-Penagos *et al.*, 2020). By contrast, Kubryakov *et al.*, (2021), working with in-situ, satellite and aerial drone photography data, discovered submesoscale eddies on the coastal zone of Crimea that generated cross-shelf transport of accumulated total suspended matter. Moreover, while it was initially suggested that offshore waters were more isotropic than near the coast (Romero *et al.*, 2013), the anisotropy associated with the persistence of a submesoscale front was also observed offshore, where Carlson *et al.*, (2018) measured Lagrangian velocities at the ocean surface by tracking the dispersion of bamboo dinner plates using novel remote sensing technology in conjunction with drifters from the LASER experiment.

Surface currents down to 100 meter scales can produce strong local dispersion of tracers and are studied for a wide range of applications, including the tracking of oceanic pollutants (Poje *et al.*, 2014). Poje and co-authors were able to describe the trajectory and the submesoscale dispersion of the Deepwater Horizon spill in the Gulf of Mexico using 300 GPS-drifters as part of the Grand Lagrangian Deployment (GLAD) program in 2012. Their results allowed the quantification of the dispersion that were until then not included in operational circulation models and satellite altimeter-derived velocity fields.

2.2.2. Vertical Processes and Transport

Submesoscale processes are known to induce enhanced vertical velocities (Klein & Lapeyre, 2009; Mahadevan, 2006; Mahadevan *et al.*, 2012) and exchanges of heat (Siegelman *et al.*, 2020; Su *et al.*, 2018, 2020), buoyancy (McWilliams, 2017) and biogeochemical tracers (Bosse *et al.*, 2017) between the mixed layer and the ocean interior. This vertical flux of tracers is responsible for the rapid stratification and of the upper ocean, which increases light exposure and residence time of phytoplankton in the euphotic layer, stimulating primary production (Lévy *et al.*, 2018; Mahadevan, 2016). The effects of submesoscale eddies associated with mixed-layer stratification were studied namely in the case of phytoplankton blooms (Brody *et al.*, 2016; Mahadevan *et al.*, 2012).

Early simulations indicated that submesoscale vertical circulations increased phytoplankton production and subduction in the open ocean (Lévy *et al.*, 2001; McGillicuddy *et al.*, 2003; Oschlies, 2002). It was later suggested that in offshore oligotrophic regime, about 20% of new primary production could be explained by submesoscale dynamics (Lévy *et al.*, 2014). This concurred with recent model simulations revealing that improved horizontal grid resolution, thus higher sensitivity to submesoscale activity, led to greater vertical transport of nutrients supporting primary production in the open ocean (Balwada *et al.*, 2018; Uchida *et al.*, 2020). Contrastingly, other studies suggest that in nutrient-rich regions such as eastern boundary upwelling systems, submesoscale currents reduce nutrient abundance from the euphotic layer, limiting primary production (Gruber *et al.*, 2011; Hauschildt *et al.*, 2021; Lathuiliere *et al.*, 2011). In the California Current System, phytoplankton abundance is particularly intensified offshore during upwelling favorable winds (Kessouri *et al.*, 2020; Shulman *et al.*, 2015).

These effects are modulated by a seasonal cycle of submesoscale motions related to the depth of the mixed layer : they are much stronger in winter, when the mixed layer is deeper due to weaker thermal stratification, than in summer, and therefore increasingly energized by baroclinic instabilities (Gula *et al.*, 2021). Evidence of this seasonality in submesoscale flows come from both numerical simulations (Ajayi *et al.*, 2021; Brannigan *et al.*, 2015; Capet *et al.*, 2008; Kessouri *et al.*, 2020; Mensa *et al.*, 2013; Sasaki *et al.*, 2014) and in-situ observations (Callies *et al.*, 2015).

Moreover, frontogenesis at the submesoscale has strong contribution to the vertical transport of tracers near the surface (Lévy *et al.*, 2012; Zhong *et al.*, 2017). Initially, vertical flows associated with submesoscale fronts were described as physical processes responsible for the supply of nutrients to the euphotic zone, modulating biological production (Williams & Follows, 2003). As a result, submesocale frontal dynamics have been widely studied over the past two decades (Capet *et al.*, 2008b; D'Asaro *et al.*, 2011; Giddy *et al.*, 2021; Lévy *et al.*, 2012; Liu & Levine, 2016). Recently, submesoscale-resolving simulations have been able to capture upwelling and downwelling patterns associated with density fronts (Hauschildt *et al.*, 2021; Jensen *et al.*, 2018) and their contribution to the vertical advection of phytoplankton (Ruiz *et al.*, 2019). In addition, submesoscale motions, through frontogenesis and baroclinic instabilities, can lead to the slumping of isopycnals and the generation of vertical density gradients in the surface mixed-layer, a process called restratification (Lapeyre *et al.*, 2006). This restratification induced by submesoscale fronts has been confirmed via in-situ observations (Johnson *et al.*, 2020; Thompson *et al.*, 2016) and models that either resolve (Lévy *et al.*, 2010; Yu *et al.*, 2019; Zhong & Bracco, 2013) or parametrize (Boccaletti *et al.*, 2007; Calvert *et al.*, 2020; Fox-Kemper & Ferrari, 2008) the submesoscale.

Much like frontogenesis, the generation of dense filaments – filamentogenesis – , form when two parallel fronts with opposite density gradients align, can also be an effect of small-scale processes (McWilliams *et al.*, 2009). The intensification of cold and dense waters at the surface can produce vertical velocities attributed to the baroclinic instabilities of the filament, reaching values of ~ 1 cm s^{-1} when submesoscale flows are resolved (Gula *et al.*, 2014). Schubert *et al.* (2021), using submesoscale-permitting simulations, showed that the Agulhas leakage, the warm and salty inflow of Indian Ocean water into the Atlantic Ocean, is increased due to strong submesoscale-induced filaments. This study highlights the importance of submesoscale flows and mixing processes on the Atlantic Meridional Overturning Circulation, and thus on the global climate.

2.3. Ocean Processes in Madeira

Mesoscale features developing around Madeira Island, particularly when originating from oceanic wakes, has been the focus of extensive research in the last two decades. Satellite images initially revealed the formation of a warm wake south of the main island of Madeira and geostrophically balanced eddies spinning off both insular flanks, with the western side being more dynamic (Caldeira *et al.*, 2002). Thereafter, ocean circulation models determined that the wake was in fact asymmetric at the ocean surface, with strong cyclonic eddies in the west and weak anticyclonic eddies in the east (Caldeira & Sangrà, 2012). This asymmetry in vorticity from Madeira's wake generation was further confirmed by a 35-year one-way coupling (atmospheric to ocean model) simulation (Alves *et al.*, 2021), which also revealed a deeper mixed-layer in the east downwelling region than in the west upwelling region, especially in the summer months. Using a similar modeling approach, Couvelard *et al.*, (2012) used a high resolution meteorological model that included Madeira's orography to force an oceanic model representing the region. This study showed that a wind-induced wake was highly contributing to the formation and containment of eddies in the lee of Madeira Island. Additionally, Caldeira *et al.*, (2014), using remote sensing data and measurements from a combination of field missions, presented the first clear evidence of a wind-induced mesoscale anticyclone in Madeira's sheltered leeward region. When comparing these results to historical records of drifter trajectories with similar spatial and temporal patterns, the authors suggested that anticyclonic eddies were regionally predominant during summer in the south of Madeira. Notwithstanding that these studies have exhaustively described Madeira's wake generation and its role in regulating mesoscale eddies, there is still a considerable lack of knowledge regarding submesoscale processes in this area.

3. Geographic Setting

Madeira is a volcanic island part of Macaronesia located in the northeast Atlantic Ocean, approximately 700 km off the western African coast (Morroco) and 850 km from the southwest Iberian Peninsula (mainland Portugal) (Fig. 1a). It is ~58 km in length and ~23 km in width and oriented in a northwest-southeast direction. Located at the eastern boundary of the North Atlantic Subtropical Gyre, intersecting the Azores Current northbound and the Canary Current eastbound, its climate is governed by the Azores subtropical high-pressure system. Madeira's high mountain ridge (reaching ~1800 m) (Fig. 1b), extending at the center and across the length of the island, is perpendicularly aligned to the incoming trade winds, which are predominately from the northeast and strongest during the summer months. This imposing orography, acting as a physical barrier to the prevailing winds, is namely responsible for the generation of atmospheric and oceanic wakes (Caldeira & Sangrà, 2012; Caldeira & Tomé, 2013; Couvelard *et al.*, 2012), which are in turn associated with high sea surface temperatures on the leeward side of the island (Caldeira *et al.*, 2002). Madeira's narrow shelf is characterized with a steep slope, and its width varies considerably, ranging between ~1 to 10 km from the shoreline (Mata *et al.*, 2013). The Madeira Archipelago also consists of the Desertas Islands and Porto Santo Island (Fig. 1b). Additionally, a submarine ridge between Madeira and the Desertas extends to 18 km in length and reaches up to 150 m in depth. Local tides are semidiurnal, with a tidal amplitude averaging 2 m (Canning-Clode *et al.*, 2008).

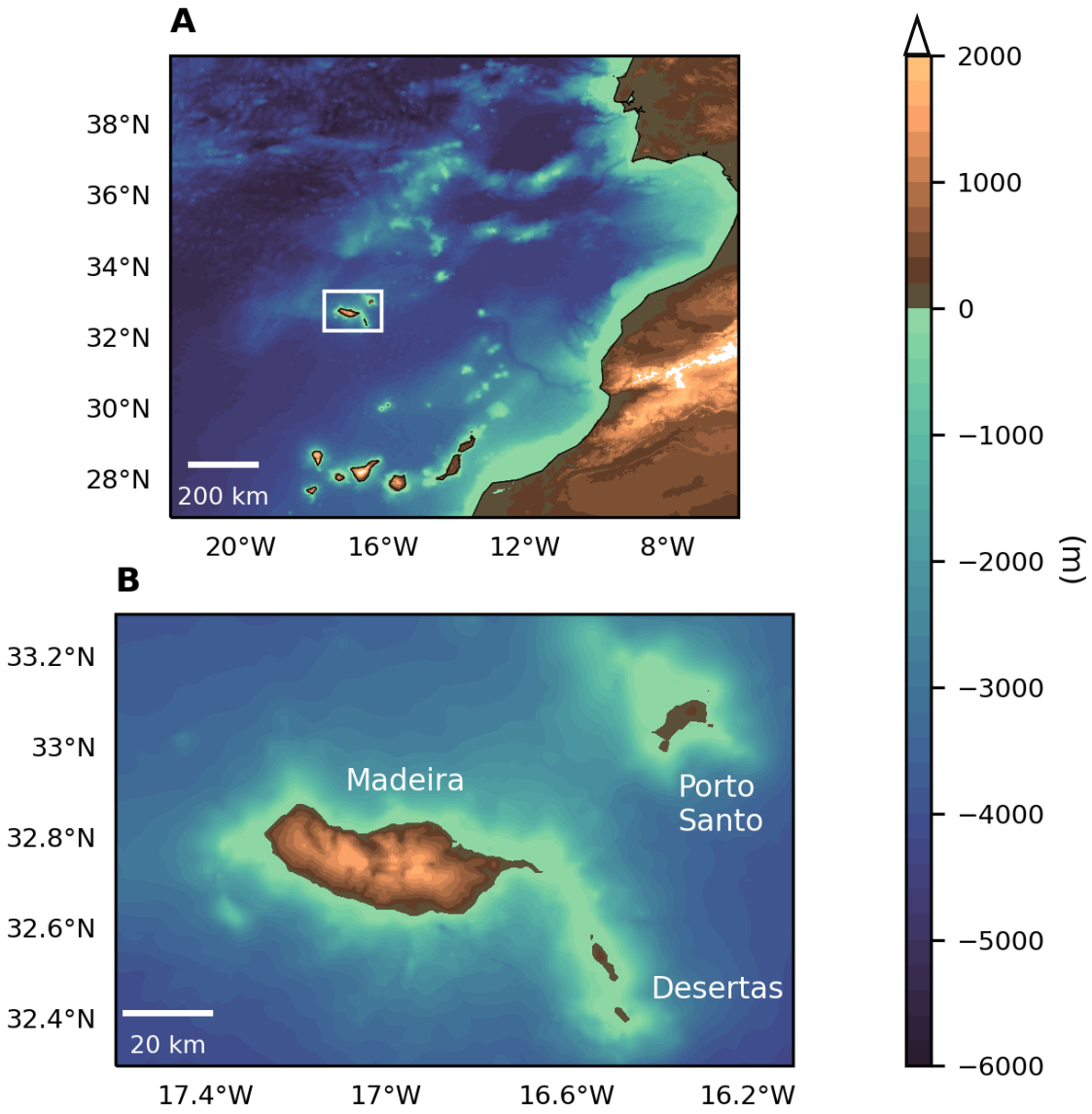

Figure 1. Topobathymetric maps of the study area. (A) Location of the Madeira Archipelago in the eastern Atlantic. The white box represents the boundaries for the ROMS and WRF models' 1 km resolution grids. (B) Madeira's island group within the extent of the 1 km resolution grid delimited in (A).

4. Data and Methods

4.1. Numerical Models

The modelling framework for this study was based on the two-way Coupled Ocean-Atmosphere-Waves-Sediment Transport (COAWST) system, which used the Regional Ocean Modelling System (ROMS) and the Weather Research and Forecasting (WRF) models for oceanic and atmospheric simulation inputs, respectively. Given the strong ocean-atmosphere interactions, this model coupling proved to be effective in recent studies on the coastal dynamics of Madeira (Alves *et al.*, 2021; Azevedo *et al.*, 2021; Pullen *et al.*, 2017). Further explanation of the COAWST model implementation can be found in (Warner et al., 2010). In this study, the ROMS and WRF models operated at a 1-km resolution, the result of a nested grid approach to improve results locally, thereby defining the spatial boundaries of the study area (Fig. 1). Numerical simulations were made using the COAWST modelling framework for the entirety of the month of July 2018, generating outputs with 1-hour time steps. A 15-day spin-up prior to July 1st was performed to ensure the stabilization and reliability of the model before producing results of the desired timeframe. From the simulation outputs, only the oceanic components and the ocean's surface layer were used for this study.

ROMS is a free-surface, terrain-following hydrodynamic model that uses primitive equations to quantitatively estimate oceanic parameters (Shchepetkin & McWilliams, 2005). For the operation of ROMS, the initial and boundary conditions were taken from the 24-hour intervals of the Mercator Ocean Model with a 1/12° resolution (Lellouche *et al.*, 2018). The input of tide conditions was parametrized based on the TPXO Global Model (Egbert & Erofeeva, 2002). The bathymetric data used as terrain for ROMS was extracted from the General Bathymetric Chart of the Oceans (GEBCO, Becker *et al.*, 2009), with a horizontal resolution of 30 arc seconds (~0.78 km).

WRF is a non-hydrostatic model useful for studying and forecasting atmospheric dynamics (Skamarock *et al.*, 2008). The initial and boundary conditions to force this model was based on the FNL (Final) Operational Model Global Tropospheric Analyses with a 6-hour interval product from National Center for Environmental Prediction (NCEP, 2000). The topography of the islands was acquired from the Shuttle Radar Topography Mission (SRTM) dataset at a 3 arc-second resolution (~90 m).

4.2. Physical Parameters

To detect general submesoscale activity in the area, Eulerian properties of flow kinematics were calculated. The Eulerian method, because it measures the instantaneous flow field, can be advantageous for its preserved spatial coverage and simple calculations. Therefore, it was deemed an adequate approach to identify small-scale and ephemerous processes within a specific domain. The following physical parameters, which have been successfully applied to characterize coastal submesoscale features in previous studies (Archer et al., 2015; Mantovanelli et al., 2017; Schaeffer et al., 2017; Zeiden et al., 2021), were selected:

Relative vorticity (ζ), defined by equation 1, has anticlockwise (>0, cyclonic) and clockwise (<0, anticyclonic) rotations in the Northern Hemisphere.

$$\zeta = \frac{\partial v}{\partial x} - \frac{\partial u}{\partial y} \quad ; \tag{1}$$

Horizontal divergence (δ) is defined by equation 2. A positive value (>0) implies locally divergent flows and upwelling, whereas a negative value (<0) represents convergence and downwelling.

$$\delta = \frac{\partial u}{\partial x} + \frac{\partial v}{\partial y} \quad ; \tag{2}$$

Total strain (ϱ), understood as the internal deformation at a given point, is defined by equation 3, which is a function of shearing strain and normal strain.

$$\varrho = \sqrt{\left(\frac{\partial v}{\partial x} + \frac{\partial u}{\partial y}\right)^2 + \left(\frac{\partial u}{\partial x} - \frac{\partial v}{\partial y}\right)^2} \quad ; \tag{3}$$

Okubo-Weiss (W), derived from Okubo (1970) and Weiss (1991), is commonly known as a parameter that informs on the relative importance of deformation and rotation. It is defined by equation 4, i.e., the difference between strain (ϱ) and rotation (ζ).

$$W = \varrho^2 - \zeta^2 \tag{4}$$

These differentiation calculations were based on the horizontal components (u, v) generated from the model outputs. To simplify their comparison, vorticity, divergence, and strain were normalized by the absolute value of Coriolis ($|f|$). Also, the ratio of ($\zeta / |f|$) estimated the Rossby number (Ro), an indicator of geostrophic balance between relative vorticity and planetary

vorticity. This *Ro* will be the parameter used in this study to evaluate the relative vorticity. The parameters were calculated using Python programming language (Van Rossum, 2009).

4.3. Forcing Scenarios

To understand the influence of different forcings on submesoscale activity, 4 separate scenarios were configured and simulated for the one-month timeframe. Scenario A recreated the most complete portrayal of ocean circulation around Madeira by including three physical forcings: wind, tides, and geostrophic processes. For simulations B-C-D, the background geostrophic forcings implemented in ROMS were forced at the model's boundaries. In scenario B, the forcing of locally generated winds was included. Scenario C excluded the wind forcing and instead considered the effect of tides. Scenario D excluded both wind and tidal forcings, thus isolating the geostrophic far-field forcing.

Scenario A, representing the most realistic version of Madeira's coastal circulation, was previously applied and validated in earlier studies (Alves *et al.*, 2021; Caldeira & Tomé, 2013). Validation of wind speed and sea level calculations were done by comparing model results with in-situ measurements of the Observatório-Funchal meteorological station and a Funchal tide gauge, respectively. This case-based methodology was inspired by an ongoing study on the insular shelf circulation in Madeira of (Reis *et al.*, in preparation).

These configurations allowed the assessment of the intensity, frequency, duration, and spatial distribution of the submesoscale-detecting parameters associated with each forcing. Once the four simulations were executed, animations of the hourly time steps were created for each parameter at the surface layer to better visualize and discern submesoscale patterns. The most relevant observations were then plotted and described in detail.

4.4. Spatio-temporal Analysis

From the different scenarios, distinct submesoscale events were identified and analyzed in depth. A detailed characterization of the spatial and temporal evolution of these submesoscale features was made using the *Ro* and *W* parameters for each of them. In addition, the surface velocity and eddy kinetic energy (EKE) were included in this analysis to further describe the identified processes over time. Horizontal velocity (V) is defined by the vector magnitude formula in equation 5.

$$V = \sqrt{u^2 + v^2} \tag{5}$$

The EKE, defined by equation 6, is a parameter used to quantify the energy generated from vortices in the ocean.

$$EKE = \frac{u^2 + v^2}{2} \tag{6}$$

These two parameters were directly calculated using the xroms package (Thyng *et al.*, 2022) made for Python which contains built-in functions for ROMS output.

5. Results

5.1. Submesoscale Activity under Different Forcing Scenarios

5.1.1. Scenario A: All Forcings

In the scenario most representative of real conditions, the parameters were visible in many areas, though mostly near the island shelf. Relative vorticity, strain and Okubo-Weiss showed significant signatures on the western, southern, and eastern margins of Madeira Island, over the Desertas ridge (<200 m depth), and on the margins of the Desertas and Porto Santo islands (Fig. 2a-c-d). Surface divergence was generally less spread out, with strong values usually found on the west and east flanks of Madeira and over the ridge (Fig. 2b).

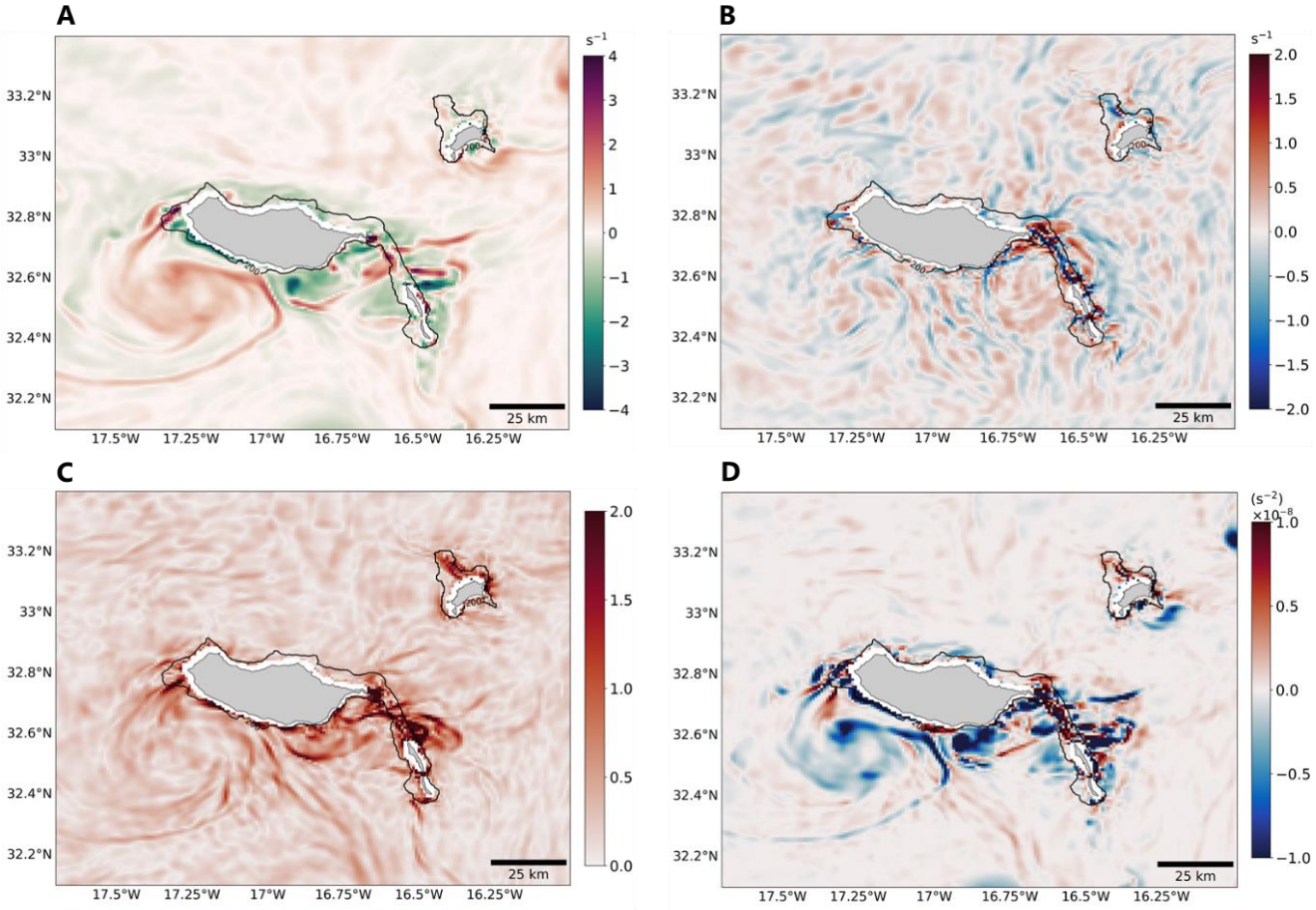

Figure 2. All parameters during scenario A. (A) Relative vorticity on 18-07 at 4:00; (B) Divergence on 14-07 at 23:00; (C) Strain on 18-07 15:00; (D) Okubo-Weiss on 18-07 at 4:00. Black line represents the 200 m isobath.

5.1.2. Scenario B: Wind Forcing

Under the wind forcing scenario, the relative vorticity parameter appeared in various locations across the archipelago. While it was mainly concentrated near coastal waters, it also showed strong values offshore.

Instances of strong vorticity were prevalent off the western and eastern flanks of Madeira Island, with more consistency in the west, as well as along the northern and southern coasts. Indeed, relatively high positive values superposed onto high negative values were persistent on the west flank (*Ro* ~4/-4), initially within the 200 m isobaths, then extending further away from the coast, for a duration of about 7 days (Fig. 3a). On the eastern side of the island, occurrences of high negative values near the coast (*Ro* ~-2) and high positive values further offshore (*Ro* ~2) were seen regularly (Fig. 3b), though not as continuously, lasting never more than one day. South of the island, instances of intense positive vorticity, with *Ro* varying between 3 and 4, manifested parallel to the coastline and lasted over 4 days (Fig. 3a-c). East of Desertas Islands, intense areas of both positive and negative vorticity (*Ro* of up to 4 and -4 respectively) appeared constantly, stretching away from shore (Fig. 3d). In Porto Santo, areas of elevated positive and negative vorticity (*Ro* ~3/-3) were observed regularly off the east and west tips of the island (Fig. b-d).

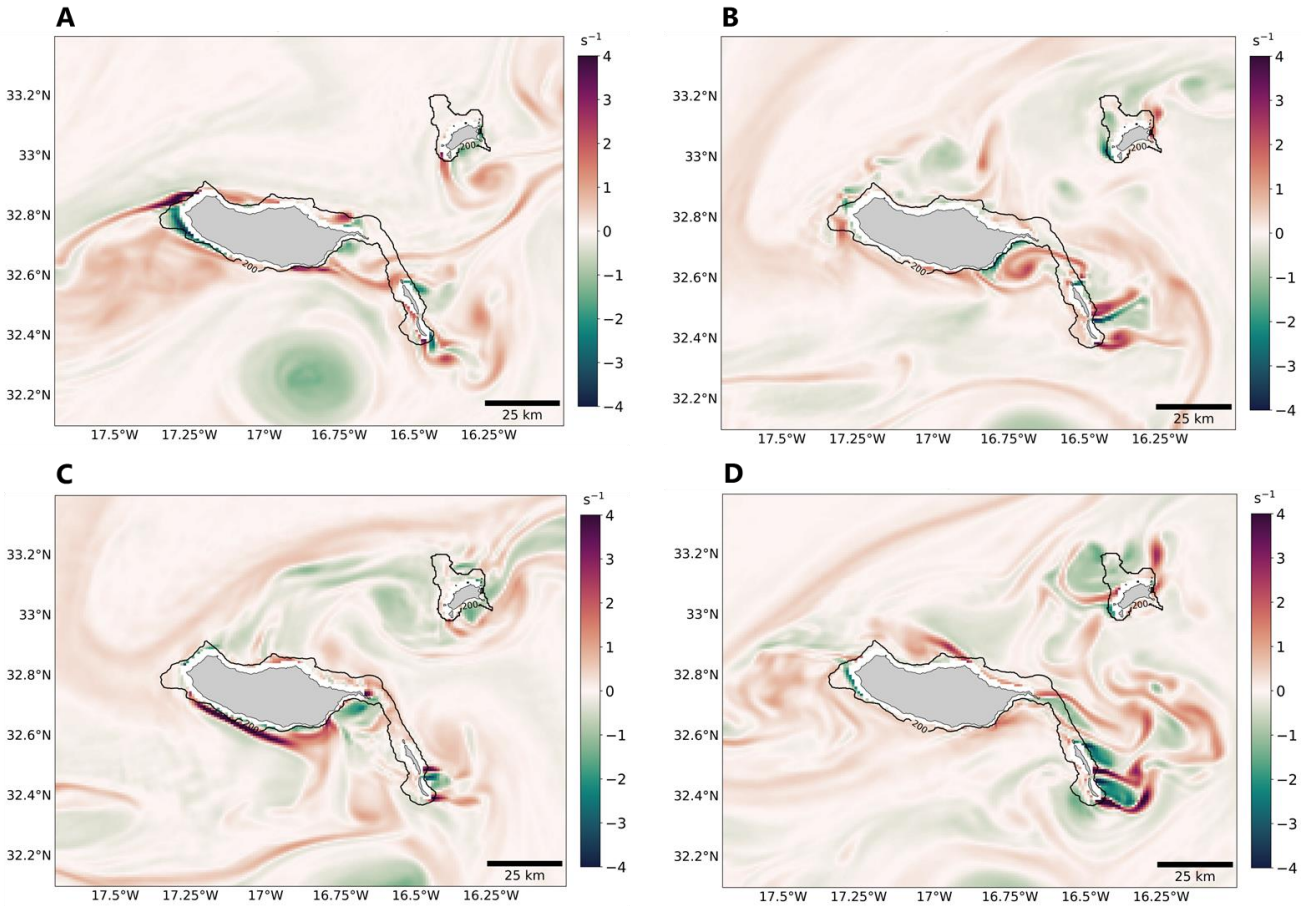

Figure 3. Relative vorticity parameter during scenario B taken on: (A) 19-07 at 10:00; (B) 04-07 at 10:00; (C) 01-07 0:00; (D) 08-07 at 17:00. Black line represents the 200 m isobath.

Surface divergence, overall, was not a significant parameter in the wind simulation, with the most notable values concentrated mainly on the western flank of Madeira Island (Fig. 4a) and over the Desertas ridge (Fig. 4b) and lasting generally only up to a few hours.

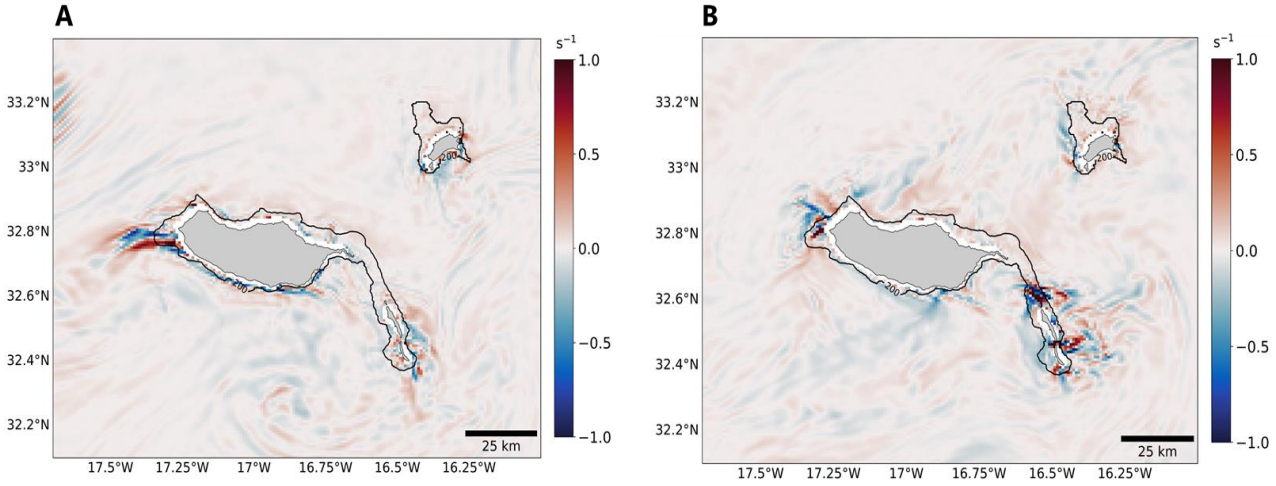

Figure 4. Divergence parameter during scenario B taken on: (A) 20-07 at 12:00; (B) 05-07 15:00. Black line represents the 200 m isobath.

Areas of high strain (ϱ of up to 2) were observed on the west tip (Fig. 5a) and along the south coastline of the main island (Fig. 5a-b). In most cases, these strained areas behaved in a similar spatial and temporal way to the areas of strong vorticity. Others occurred recurrently North and East of the Desertas (Fig. 5c).

Regarding the W parameter, zones of relatively elevated negative values were prevalent across the study area under the isolated wind forcing. This was particularly the case by Madeira's western (Fig. 6a) and southern (Fig. 6b) shores, as well as on the margins of the Desertas and Porto Santo islands (Fig. 6c). Constant negative W in Madeira's west and south coasts and around the Desertas, where high values of both vorticity and strain were observed, indicated a clear dominance of rotation over strain in these areas.

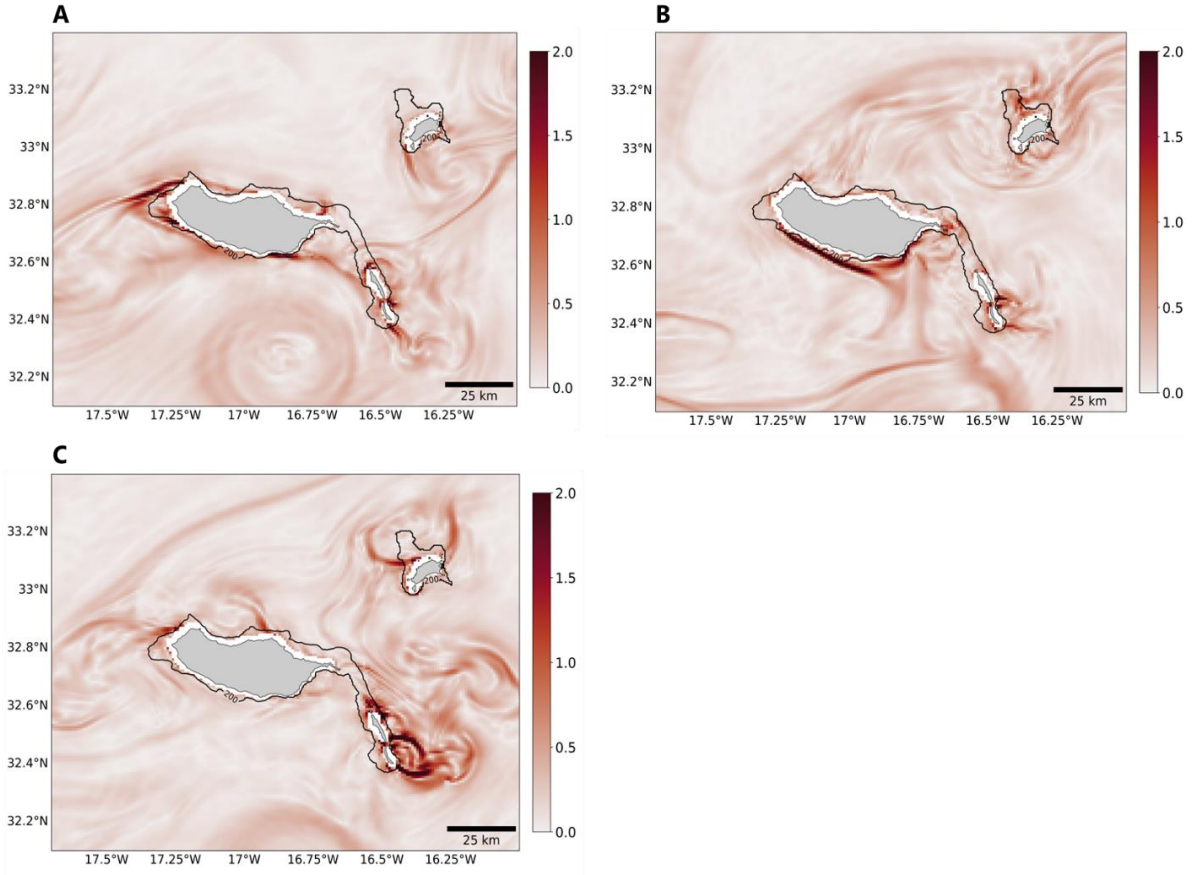

Figure 6. Strain parameter during scenario B taken on: (A) 19-07 at 18:00; (B) 01-07 0:00; (C) 09-07 5:00. Black line represents the 200 m isobath.

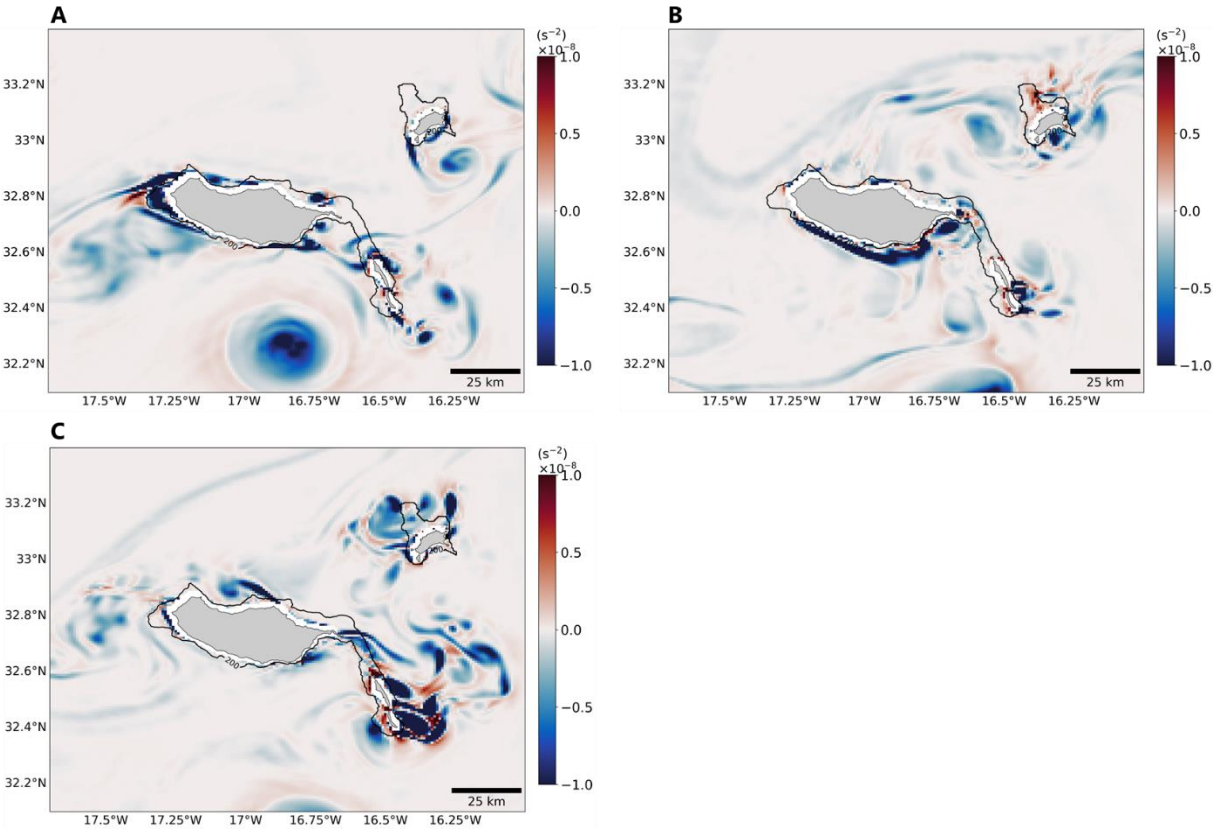

Figure 5. Okubo-Weiss parameter during scenario B taken on: (A) 19-07 at 16:00; (B) 01-07 0:00; (C) 08-07 16:00. Black line represents the 200 m isobath.

5.1.3. Scenario C: Tidal Forcing

When tides were isolated, the parameters were generally more intense in shallow or coastal waters than in deeper waters. The vorticity parameter mainly showed high values (*Ro* of ~ 4/-4) along the eastern tip of Madeira Island and North of Desertas Islands (Fig. 7a-b). These areas were characterized by east-west moving patterns with periods of about 12 hours. Also, occasional clumps of negative vorticity with a *Ro* of around -2 formed along the south coast of Madeira and remained near the shelf for approximately 1 day (Fig. 7b). On the southeastern margins of Porto Santo Island, other areas with high Rossby numbers (*Ro* of ~ 4/-3) were observed, where both positive and negative vorticity were generated (Fig c).

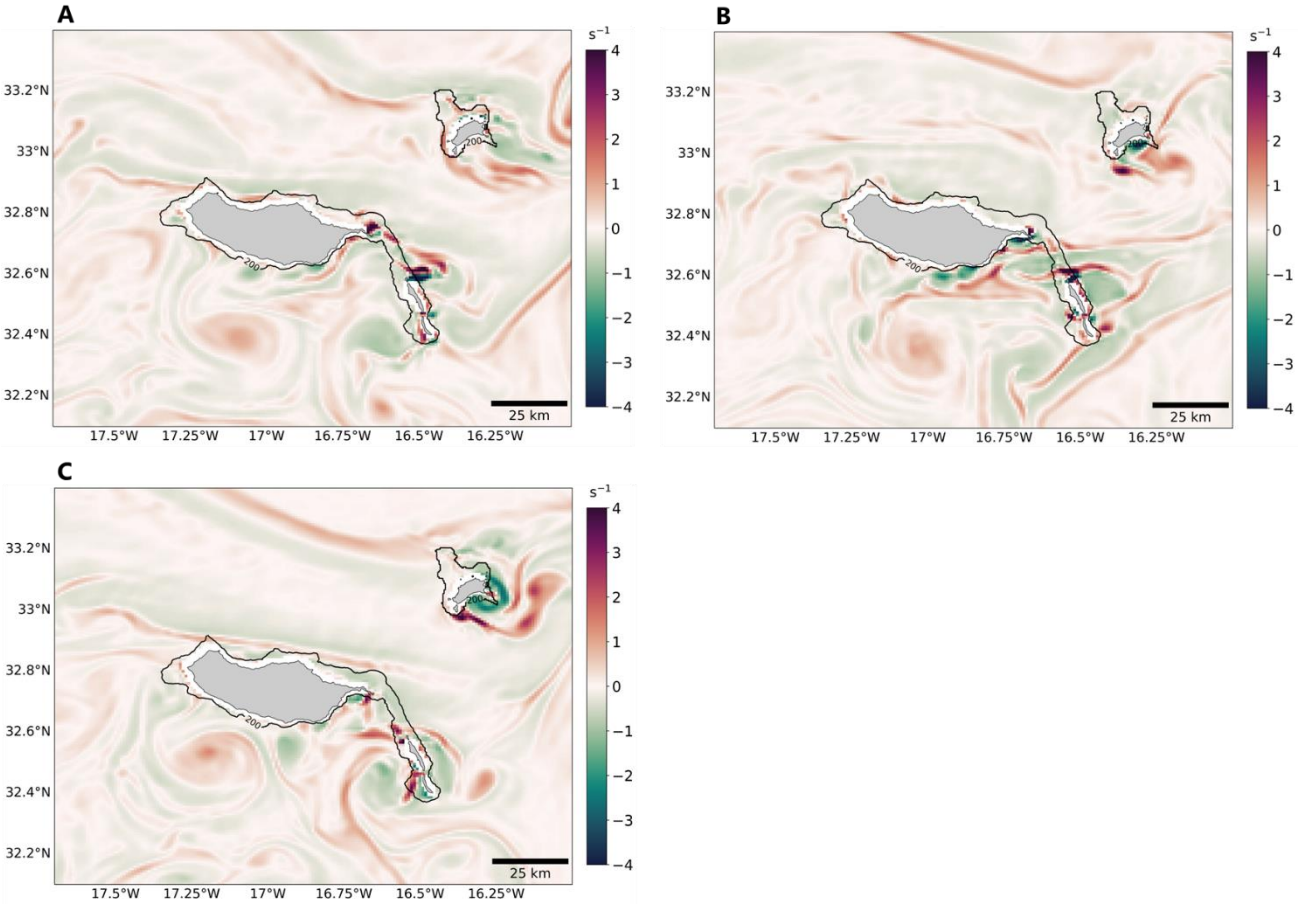

Figure 7. Relative vorticity parameter during scenario C taken on: (A) 19-07 at 10:00; (B) 04-07 at 10:00; (C) 01-07 0:00; (D) 08-07 at 17:00. Black line represents the 200 m isobath.

Moreover, zones of strong surface convergence (δ of -2) were periodically found over the Desertas Ridge (<200 m depth) (Fig. 8a). Equally in periods of 12 hours, adjacent strips of relatively high convergence and divergence (δ of -1/1 respectively) drifted westwards parallel to the ridge (Fig. 8b).

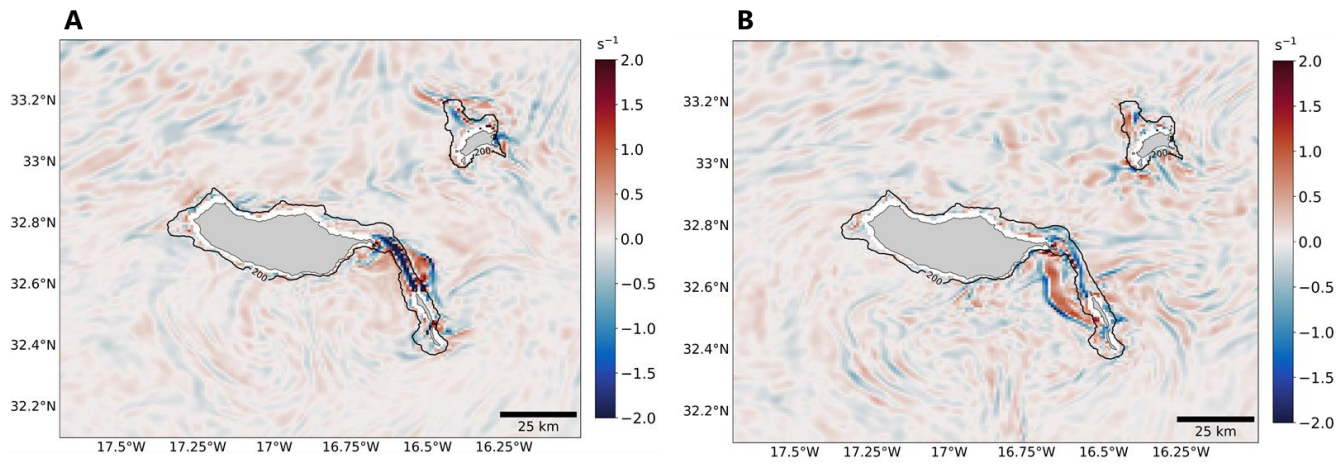

Figure 8. Divergence parameter during scenario C taken on: (A) 26-07 at 23:00; (B) 21-07 0:00. Black line represents the 200 m isobath.

Furthermore, considerably high values of strain (ϱ of up to 2) were regularly observed over the Desertas ridge and very near the eastern and southeastern shores of Madeira (Fig. 9a). The Porto Santo surroundings did not show consistent strained areas, but when they did, they appeared mostly south of the island and lasted up to 12 hours (Fig. 9b).

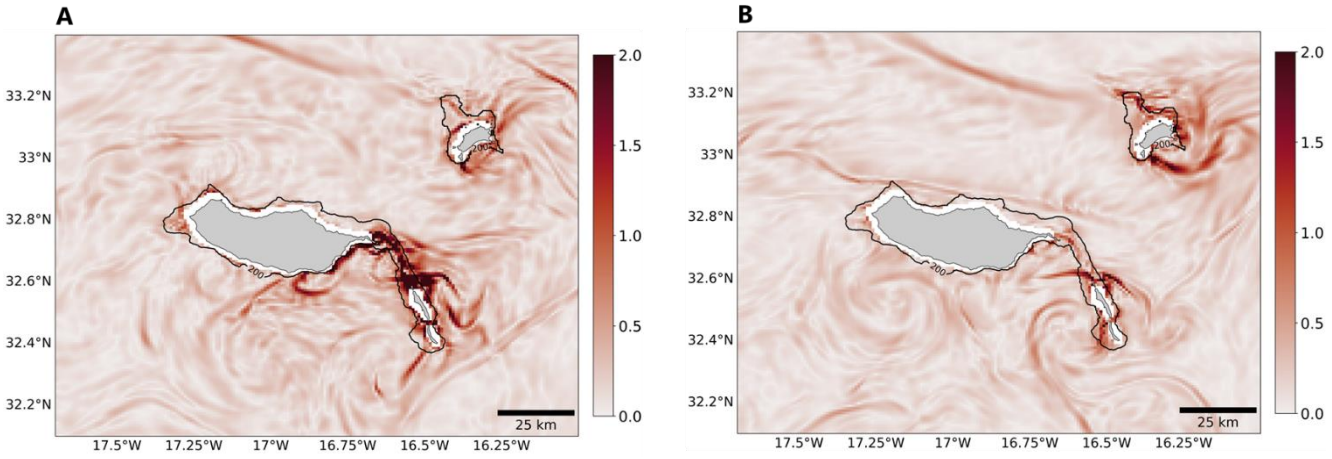

Figure 9. Strain parameter during scenario C taken on: (A) 16-07 at 13:00; (B) 08-07 6:00. Black line represents the 200 m isobath.

The *W* parameter alternated between significantly high positive and negative values over the ridge, but more often showed high positive indices (Fig. 10a), corresponding to a strain dominance over rotation. Near Porto Santo, off the south and east coasts, there was instead a large dominance of rotation over strain, dictated by predominant negative values (Fig. 10b).

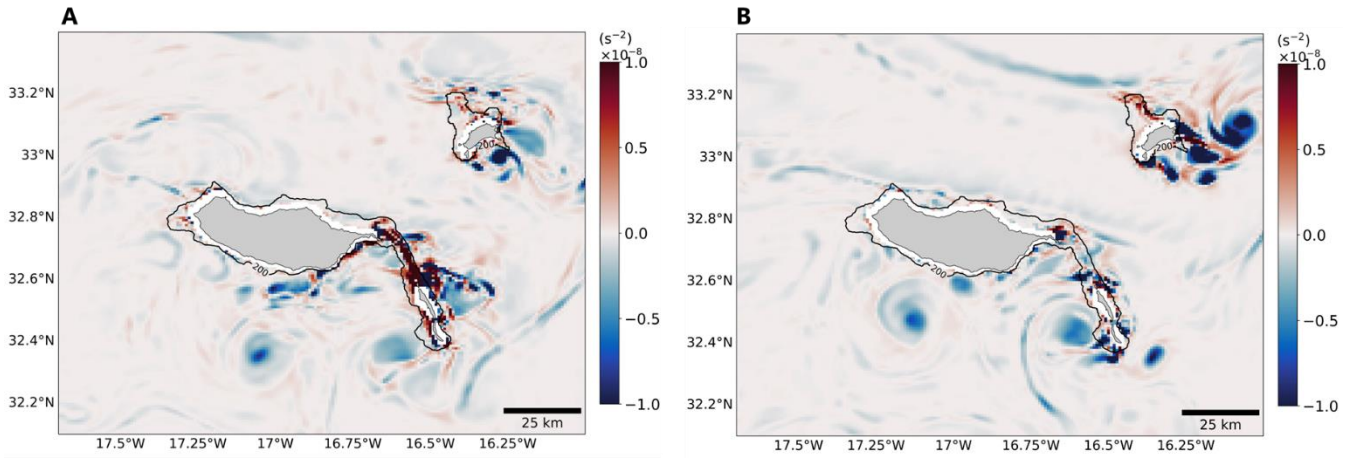

Figure 10. Okubo-Weiss parameter during scenario C taken on: (A) 15-07 at 0:00; (B) 10-07 0:00. Black line represents the 200 m isobath.

5.1.4. Scenario D: Geostrophic Forcing

In the geostrophic forcing scenario, the parameters were generally more noticeable nearshore, but manifested offshore as well.

Significantly high vorticity occurred all around Madeira Island as well as East of Desertas Islands. Along the north coast, adjacent areas of moderately high positive and negative vorticity (*Ro* ~ 2.5/-2.5) were regularly observed (Fig. 11a) for several hours. Additionally, marked features of negative vorticity were intensifying up to a *Ro* of -4 at the tip of Ponto de São Lourenço, from where they continued moving along the southeastern shore (Fig. 11b). Along the southeastern margins of the island, various areas with a *Ro* of about 3 were seen forming and lasting from 3 to 6 days (Fig 11a-c). On the northwest coast, instances of strong positive (*Ro* ~ 3) (Fig. 11b) and negative vorticity (*Ro* ~-4) (Fig. 11c) were observed. The former spread thinly towards the west, similarly to the strip of positive vorticity identified in the wind scenario (Fig. 3a) which persisted for a week, while the latter had northward movement and spread wider, lasting for approximately 3 days. Furthermore, on the eastern coastal area of the Desertas, considerably high values of negative vorticity (*Ro* ~-4) eventually gave way to anticyclonic eddies of up to 7km in diameter (Fig. 11d). These eddies (*Ro* ~-1) propagated north towards Porto Santo and were active for over 4 days.

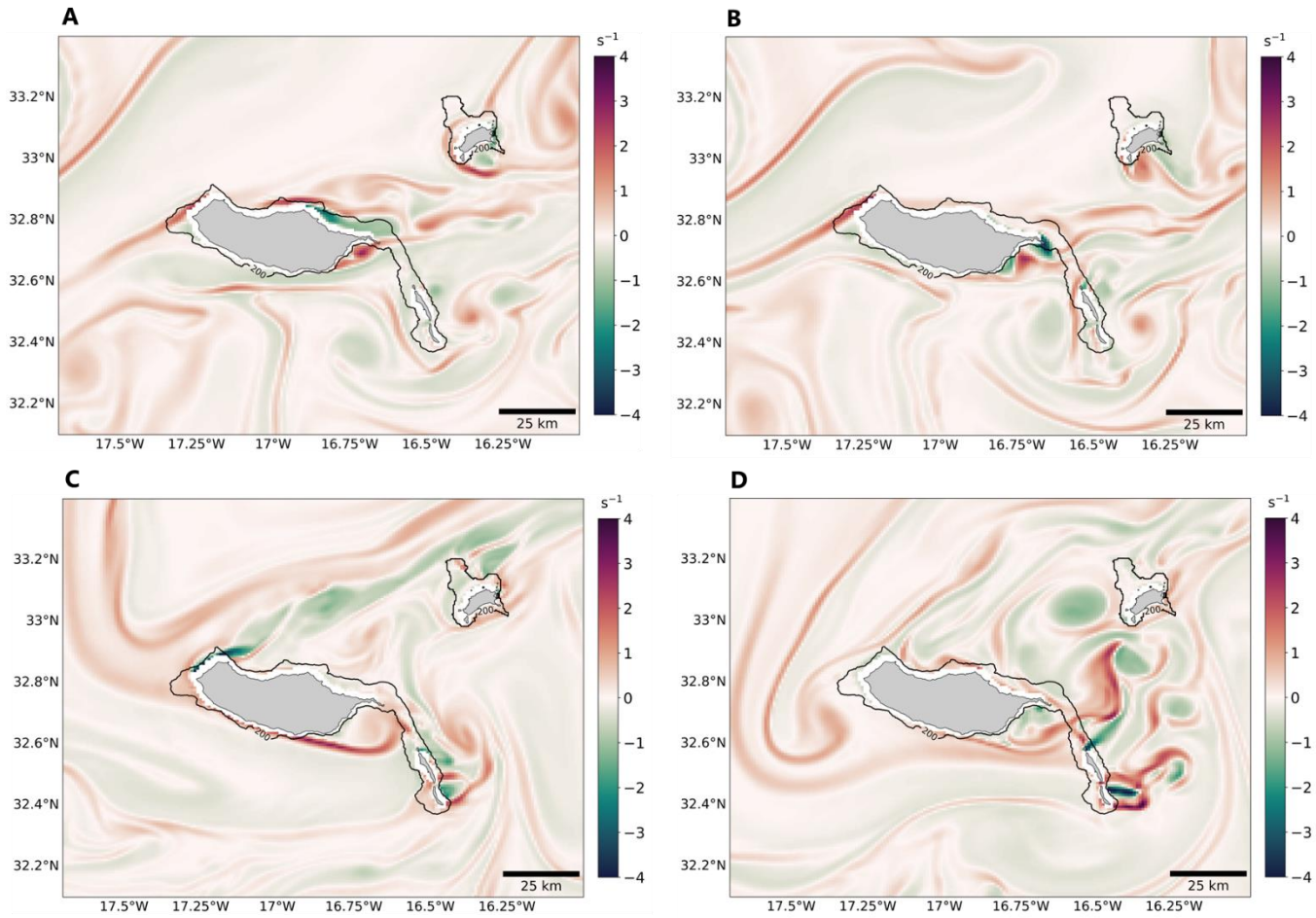

Figure 11. Relative vorticity parameter during scenario D taken on: (A) 18-07 at 11:00; (B) 20-07 at 13:00; (C) 01-07 0:00; (D) 06-07 at 0:00. Black line represents the 200 m isobath.

The divergence parameter only showed two significant areas of activity: by the east tip of Madeira (Fig. 12a) and over the Desertas ridge (Fig. 12b), where adjacent areas of both divergence and convergence were consistently observed.

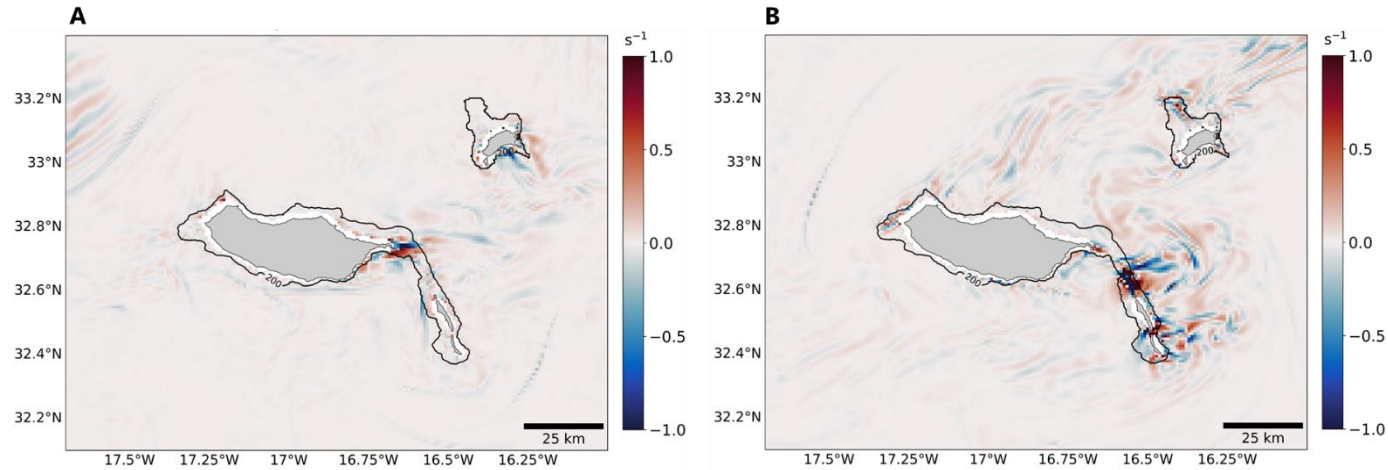

Figure 12. Divergence parameter during scenario D taken on: (A) 19-07 at 23:00; (B) 04-07 22:00. Black line represents the 200 m isobath.

Areas of considerably high strain (ϱ of up to 2) were notably apparent around Madeira on its northwestern and southeastern (Fig. 13a-b) margins, as well as along its northern coast (Fig. 13c). South-East of the Desertas Islands, recurrent occurrences of high strain ($\varrho \geq 2$) were seen off the coast, while others were also visible over the ridge (Fig. 13d).

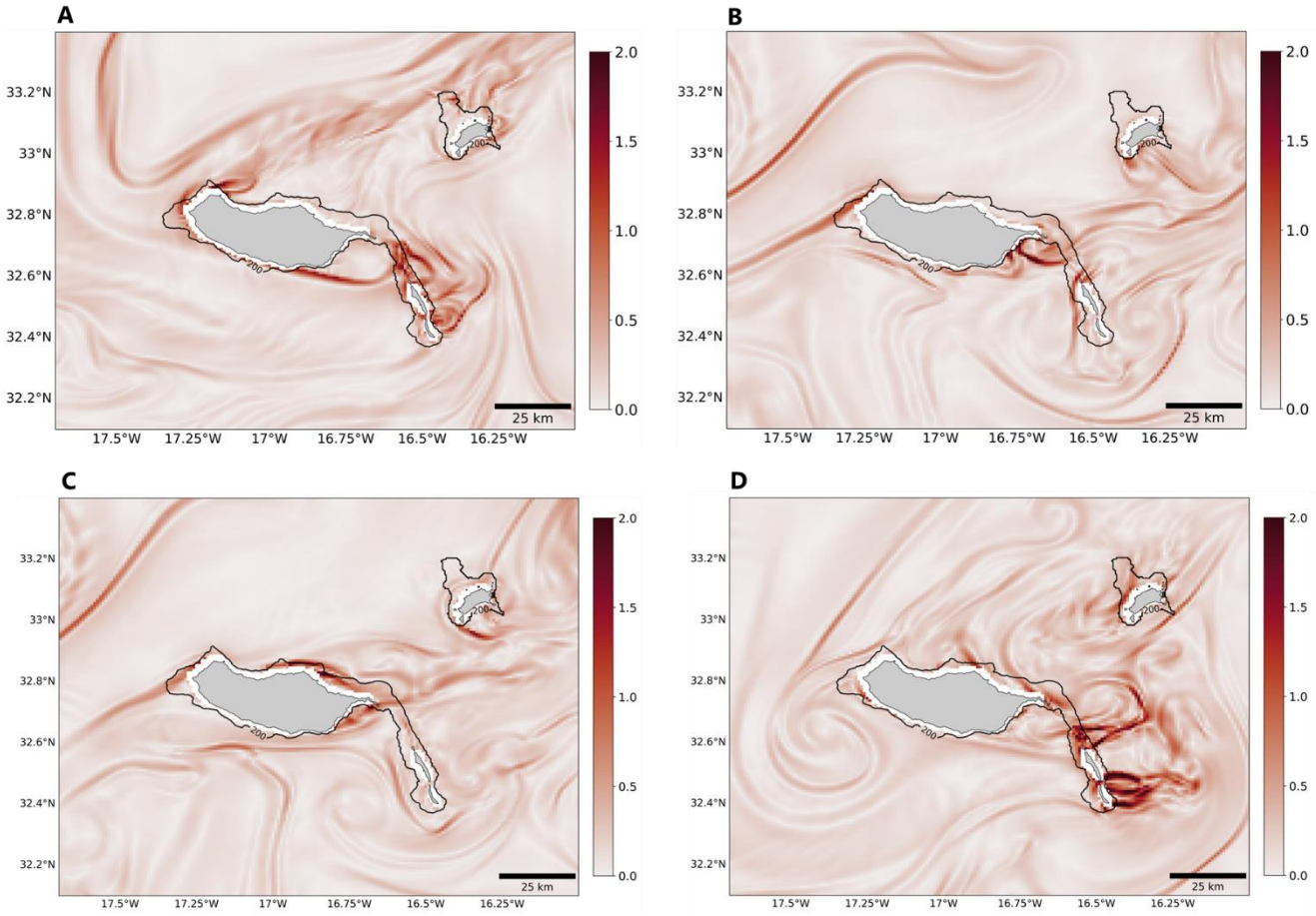

Figure 13. Strain parameter during scenario D taken on: (A) 1-07 at 18:00; (B) 20-07 20:00; (C) 18-07 15:00; (D) 07-07 at 15:00. Black line represents the 200 m isobath.

Finally, high negative values of W were observed in the same areas of vorticity and strain (Fig. 14), indicating once more a general tendency of a higher rotation over strain ratio.

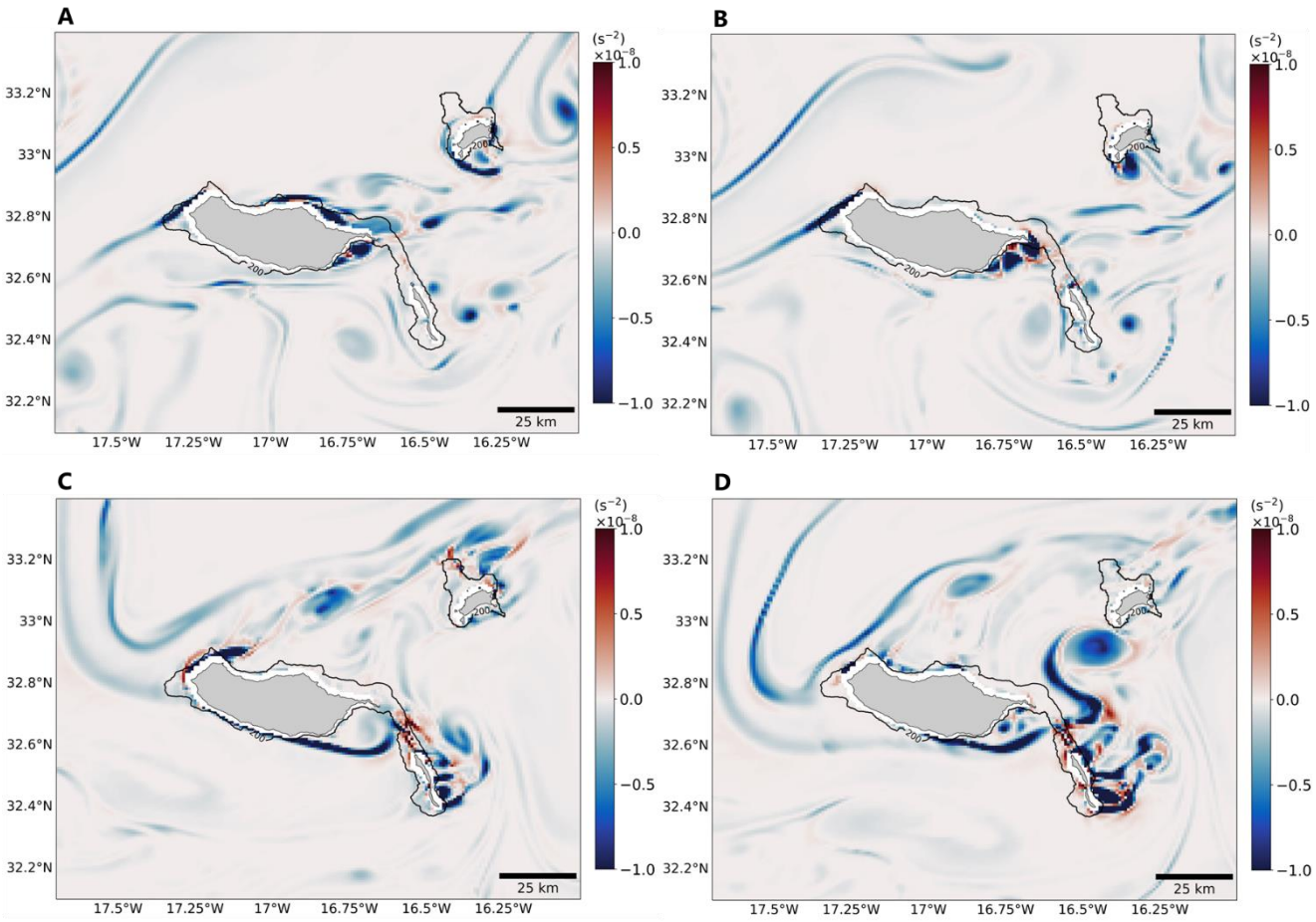

Figure 14. Okubo-Weiss parameter during scenario D taken on: (A) 18-07 at 14:00; (B) 20-07 14:00; (C) 01-07 8:00; (D) 04-07 at 0:00. Black line represents the 200 m isobath.

5.2. Spatio-temporal Analysis of Submesoscale Features

5.2.1. All Forcings Scenario

In the simulation combining all forcings, a submesoscale process was located on Madeira's south coast. On July 18, the feature manifested along the 1000 m isobath (Fig. 15a-d-g-j). The following day, on the 19th, a 12-km wide anticyclonic eddie was created, with considerably strong negative values of vorticity (*Ro* ~-2.5) and Okubo-Weiss ($W \leq -1x10^{-8}$), and a surface velocity of up to 0.6 m/s (Fig. b-e-h-k). As it expanded (~15-km diameter at its peak), the eddie travelled slightly offshore towards the South-East but overall remained relatively near its original position, while being active for over 3 days (Fig. c-f-i-l). In relation to the values of the other parameters, the EKE was noticeably low within the vortex area through the entirety of the process (Fig. j-k-l).

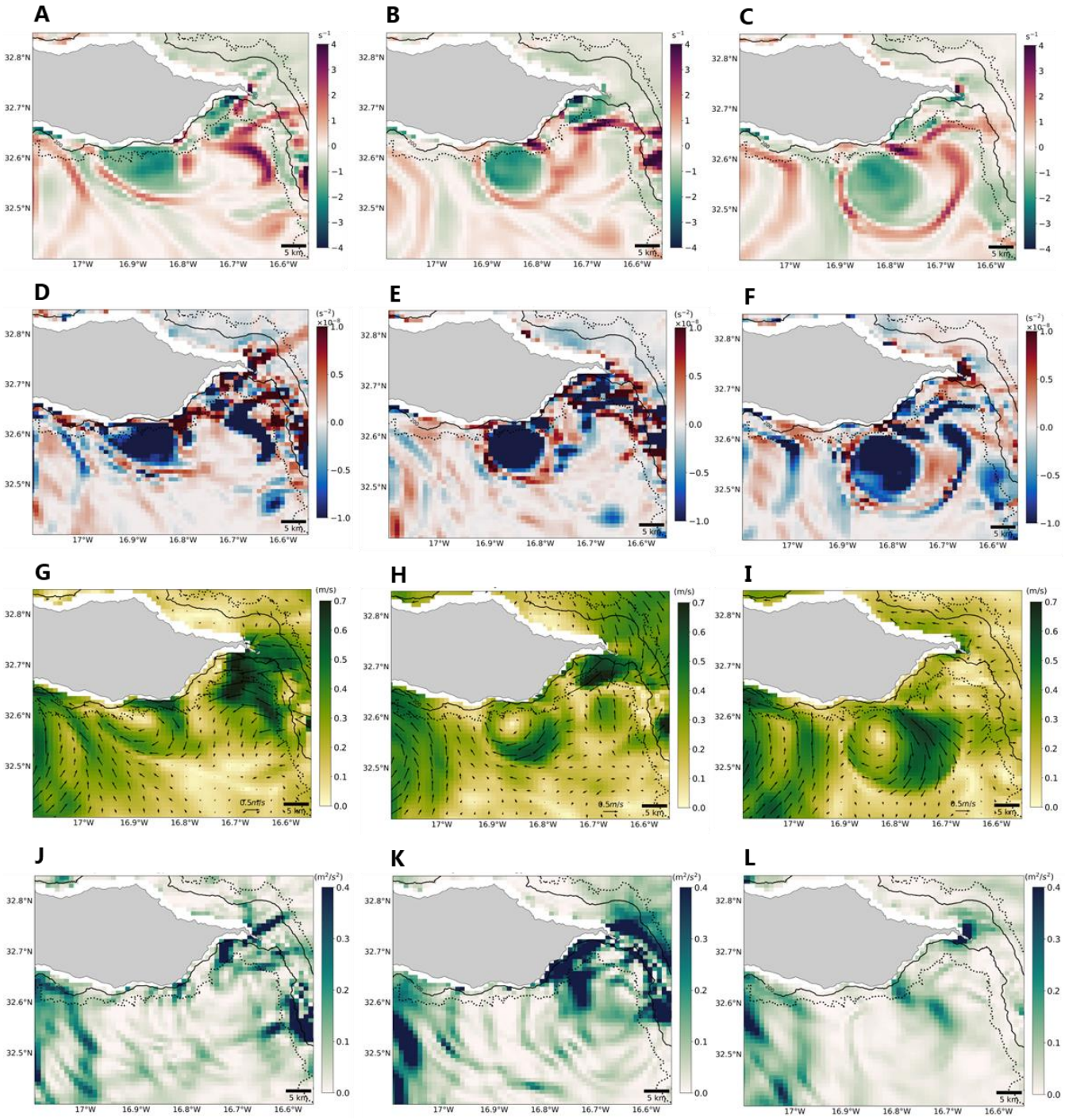

Figure 15. Submesoscale episode from scenario A, featuring vorticity (A-B-C), Okubo-Weiss (D-E-F), velocity (black arrows are instantaneous vectors at every third point) (G-H-I), and eddy kinetic energy (J-K-L). Left panels were taken on 18-07 at 20:00, center panels on 19-07 at 12:00, and right panels on 22-07 at 19:00. Black full line represents the 200 m isobath, and the black dotted line represents the 1000 m isobath.

5.2.2. Wind Forcing Scenario

Two distinct events were detected during the wind scenario, both featuring what seemed to be submesoscale eddies located on the southeast and north coasts of Madeira Island. They occurred after an intense period of positive vorticity, which started around July 19 and grew in intensity for several days, reaching Rossby numbers of approximately 3.5 (SE) and 2.5 (N) (Fig. 16).

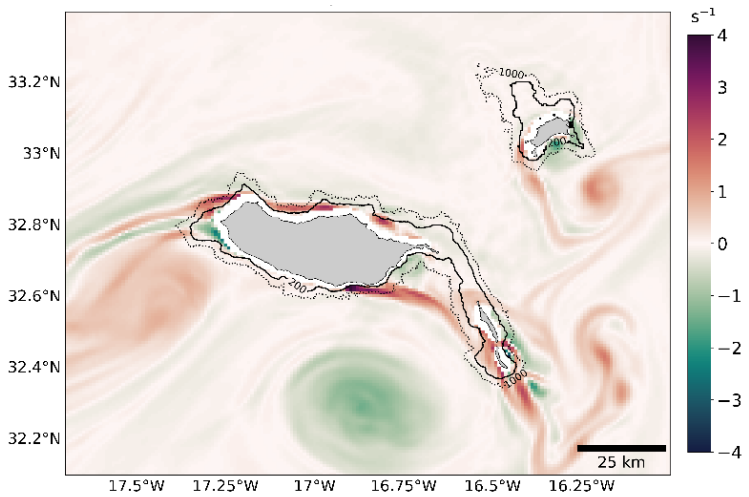

Figure 16. Average relative vorticity during July 19-23 from scenario B. Black full line represents the 200 m isobath, and the black dotted line represents the 1000 m isobath.

In the South-East, a long strip of persistent positive vorticity and negative *W* (rotation dominance) extended to the Desertas Islands. Then, from July 23, the strip got disrupted and formed a series of cyclonic eddies with diameters ranging from 3 to 5 km (Fig. 17a-c-e-g). These eddies propagated beyond Madeira's 1000 m isobath and towards the west coast of the Desertas, each lasting between 1-2 days. (Fig. 17b-d-f-h). They started with a *Ro* of around 3 (Fig. 17a) and lowered in vorticity intensity towards their end with a *Ro* between 1 and 2 (Fig. 17b). The EKE associated with these features reached approximately 0.25 m^2/s^2 (Fig. 17g-h). Moreover, these submesoscale eddies were located on the northeastern fringes of a much larger process which possessed an area of relatively similar surface velocity (>0.5 m/s) (Fig. 17e-f). This large feature seemed to be an anticyclonic mesoscale eddie given its very wide radius and clockwise rotation.

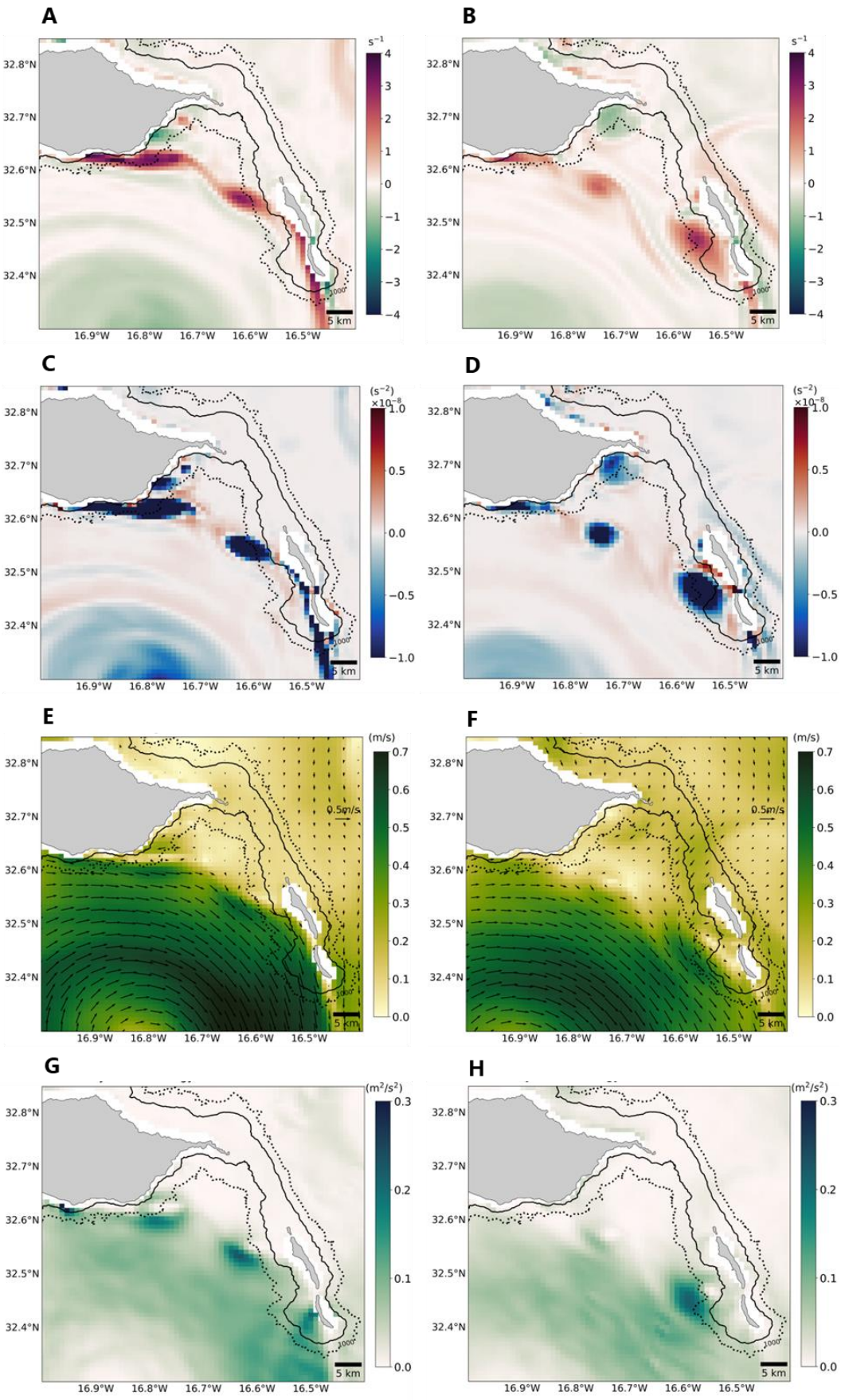

Figure 17. Submesoscale episode from scenario B, featuring vorticity (A-B), Okubo-Weiss (C-D), velocity (black arrows are instantaneous vectors at every third point) (E-F), and eddy kinetic energy (G-H). Left panels were taken on 23-07 at 10:00, right panels on 25-07 at 18:00. Black full line represents the 200 m isobath, and the black dotted line represents the 1000 m isobath.

On the north coast, two cyclonic eddies of approximately 3 km wide were formed on July 24 (Fig. 18a-d-g-j) and advanced eastwards along the 1000 m bathymetric line (Fig. 18b-e-h-k). They eventually reached northeast of Madeira and the Desertas Islands, respectively (Fig. 18d-f-i-l) and lasted over 6 days. These small-scale eddies started with a *Ro* of around 2 (Fig. 18a) and finished their journey with a *Ro* lower than 1 (Fig. 18c), while also declining in *W*, velocity, and EKE over time. Despite their weakening signatures throughout the event, these eddies were more discernable, longer lasting, and closer to the shelf than the previous set of eddies which ventured further away from the shelf (Fig. 17).

5.2.3. Geostrophic Forcing Scenario

Another submesoscale episode was identified in the isolated far-field forcing simulation. On the northeast coast of Madeira, an intense and elongated area of positive vorticity (*Ro* of ~3) and negative *W* was spotted on July 10 in very shallow waters (< 200 m depth) (Fig. 19a-d-g-j). This feature was created on the edges of a larger, mesoscale process, which appeared to have been an anticyclonic eddie due to its negative vorticity and clockwise rotation (Fig. 19b-e-h-k). The smaller-scaled process initially went in a northward direction. Then, on July 14, an 11-km wide cyclonic eddie (counterclockwise rotation) was formed over and beyond the 1000 m bathymetric line (Fig. 19c-f-i-l) and was directed eastward for a duration of 2 days. During its propagation, this eddie had a *Ro* of approximately 1.5 (Fig. 19c), a $W \leq -1x10^{-8}$ (Fig. 19f), a surface velocity of about 0.3 m/s (Fig. 19i) and an EKE nearing 0.1 m^2/s^2 (Fig. 19l).

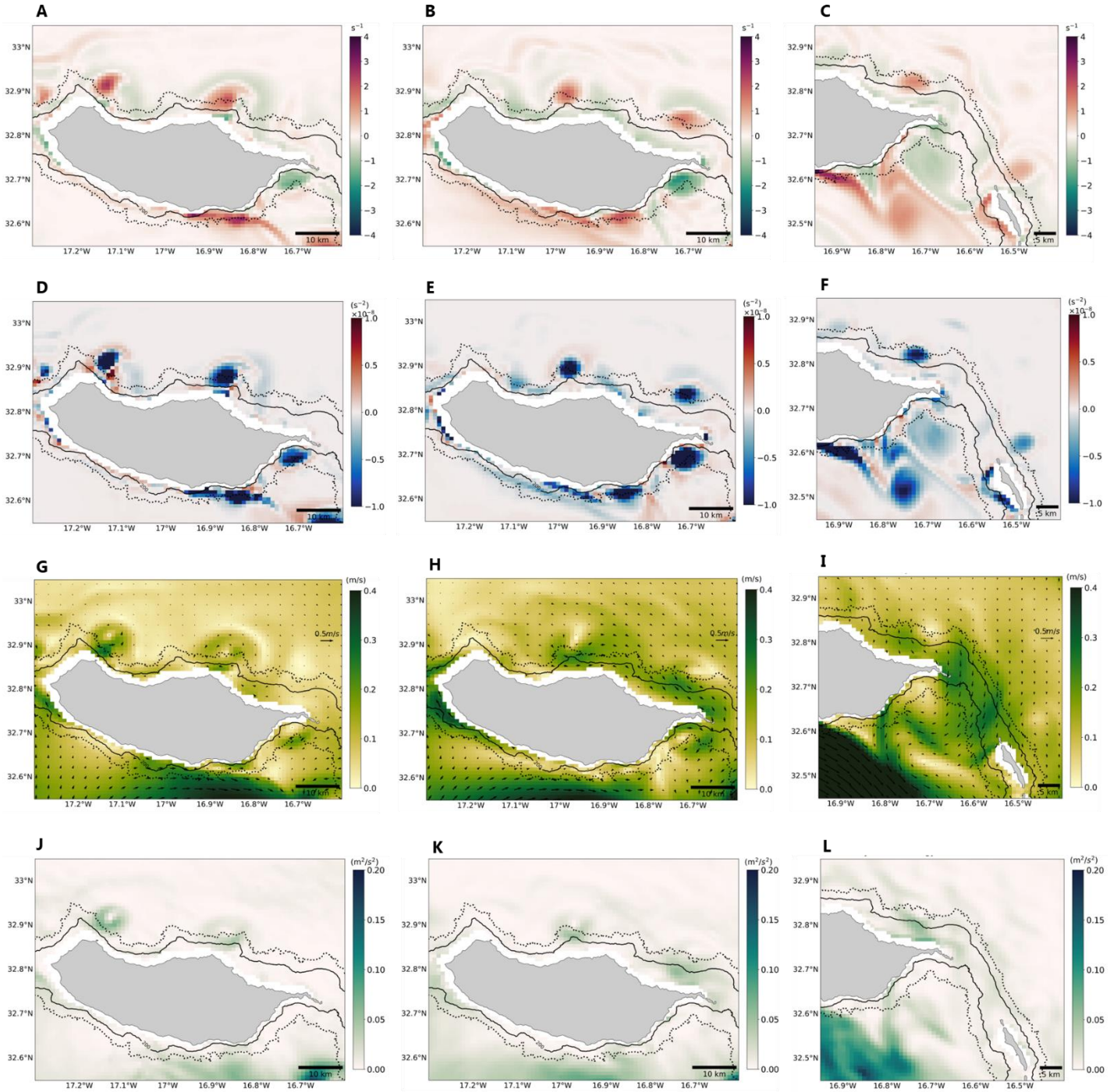

Figure 18. Submesoscale episode from scenario B, featuring vorticity (A-B-C), Okubo-Weiss (D-E-F), velocity (black arrows are instantaneous vectors at every third point) (G-H-I), and eddy kinetic energy (J-K-L). Left panels were taken on 24-07 at 22:00, center panels on 27-07 at 8:00, and right panels on 30-07 at 18:00. Black full line represents the 200 m isobath, and the black dotted line represents the 1000 m isobath.

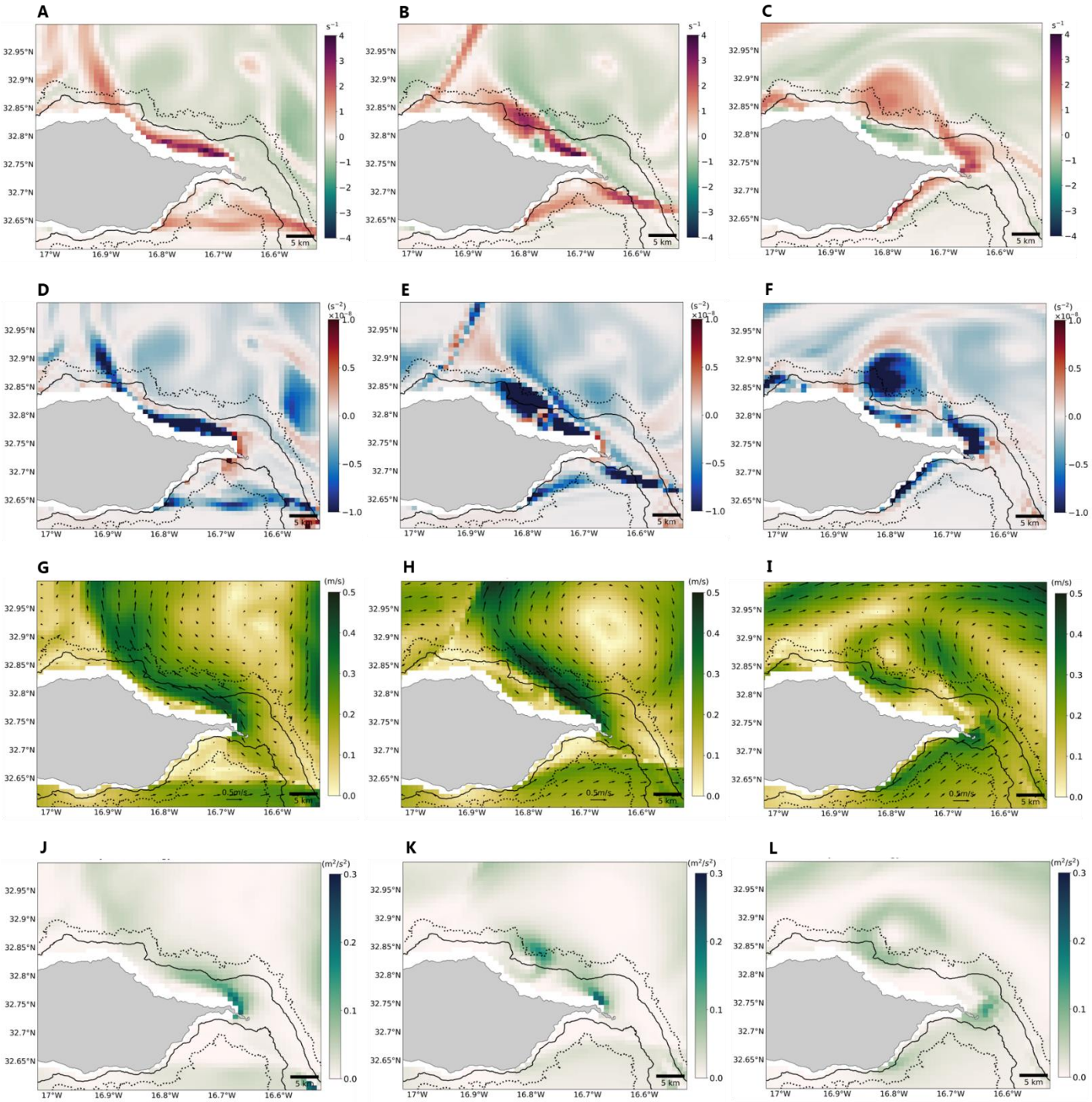

Figure 19. Submesoscale episode from scenario D, featuring vorticity (A-B-C), Okubo-Weiss (D-E-F), velocity (black arrows are instantaneous vectors at every third point) (G-H-I), and eddy kinetic energy (J-K-L). Left panels were taken on 10-07 at 23:00, center panels on 12-07 at 16:00, and right panels on 14-07 at 19:00. Black full line represents the 200 m isobath, and the black dotted line represents the 1000 m isobath.

6. Discussion

For all scenarios, the highest values for all parameters were mainly found close to the shore, near 200 m depth. This concurs with the conclusions of Reis et al. (in preparation), stating that there is a current shear between the inshore and offshore circulation. Therefore, the majority of submesoscale activity occurred over or near Madeira's shelf. However, the spread of this activity still varied between the isolated-forcings scenarios. For instance, in scenarios B and D, parameters showed more sparse values across the domain than in scenario C, indicating significant activity further offshore as well. This is likely due to generally higher wind speed and geostrophic velocity variability in both duration and intensity. Contrastingly, in scenario C, submesoscale processes were concentrated in shallow waters. Significant activity was particularly observed over the Desertas ridge, which coincides with the strong tidal signature in that area (Reis et al., in preparation). In addition, scenario C featured the most periodical instances for all parameters, most likely due to the influence of semidiurnal tides in the region. In turn, less irregularities associated with submesoscale turbulent flows were found in this scenario. Moreover, simulations B and D featured more irregular and persistent events, therefore suggesting a greater influence on submesoscale activity. In fact, similar patterns in comparable timeframes were observed between these two scenarios. For example, a strip of high positive vorticity located northwest of Madeira was seen during the same time in both cases (Fig. 3a, 11b). This pattern is related to the island's western tip-jet, which is caused by the constant northeasterly winds (Miranda et al., 2021) and characterized by geostrophic flow (Alves et al., 2020), thereby explaining its appearance under both wind and geostrophic forcing simulations. Furthermore, there was a clear dominance of rotation over strain in both scenarios B and D, whereas scenario C was rather strain-dominated, particularly over the ridge, where currents presumably experience higher bottom friction as a result of the shallow sea floor.

In the spatio-temporal analysis, eddies were the only detected submesoscale feature. The Okubo-Weiss parameter showed stronger negative values in the cores and relatively weaker positive values in the edges, further associating these patterns to an ocean eddie regime (Mcwilliams, 1984). The *Ro* values associated with these eddies ranged from ~|1| to |2.5|, which compare to submesoscale eddies with Ro values of $O(1)$ located near the deep-sea island of Palau (Johnston et al., 2019; Zeiden et al., 2021). However, these values are slightly lower than those previously obtained in July near Madeira (*Ro* ~|4|) from a similar numerical study

(Couvelard et al., 2012). Eddies observed in all scenarios had eastward movement, which is likely due to the geostrophic flow coming mainly from the West during the summer months (Caldeira & Sangrà, 2012). No distinct submesoscale feature was detected in scenario C (tidal forcing), which disagrees with previous studies who found submesoscale tidal eddies in the wake of islands (Delandmeter et al., 2017; MacKinnon et al., 2019). Although, the former obtained fine-scaled vortices as small as 10-20 m in size by largely increasing grid resolution up to 50 m near the coast, while the latter measured ~1 km eddies from in-situ instruments aboard a ship. In comparison, this present study was unable to resolve features at such small scales.

In scenario A, which considered all forcings, the coherent anticyclonic eddie spotted southeast of Madeira is consistent with the historical tendency of finding anticyclonic vortices leeward of the island's east flank, which are primarily due to the wake phenomenon (Alves et al., 2020; Caldeira & Sangrà, 2012; Couvelard et al., 2012). In fact, it was originally demonstrated with remote sensing and numerical modelling that island wakes were commonly generating submesoscale eddies in the upper ocean, notably in the Southern California Bight (Caldeira et al., 2005; Dong & McWilliams, 2007). Observational evidence of small-scale eddies was later provided in various island wake areas, including Lanai Island, Hawaii (Dong *et al.*, 2009), the Juan Fernández archipelago (Andrade *et al.*, 2014), Green Island, Taiwan (Chang *et al.*, 2013), and, more recently, Palau (Johnston et al., 2019). Thus, this simulated anticyclone may very well be induced by Madeira's wake processes, which are typically strong during summer (Caldeira et al., 2002; Couvelard et al., 2012). Moreover, the very limited propagation of this eddie from its coastal inception corresponds to the behavior of previously registered drifter trajectories, which were generally maintained over the insular shelf (Reis et al., in preparation). In addition, this suggests the possibility for this eddie to retain particles that follow the alongshore circulation established by the former study. This material retention near the shelf would be in accordance with Bolado-Penagos et al. (2020), who linked the interaction of coastal flows and submesoscale structures with higher chl-a residence time. Ultimately, since it evolved in the most realistic conditions, this eddie can be determined as the most reliable submesoscale feature among all observed herein.

Smaller cyclonic eddies found in the wind-driven scenario B (Fig. 17) occurred in a similar area than in scenario A (Fig. 15). This is in agreement with Alves et al. (2021) who, by forcing

atmospheric fields on an ocean simulation, concluded that Madeira's east tip-jet, being perpendicular to the island, reinforces the formation of shedded vortices. It is, however, inconsistent with their calculations of a predominantly negative mean vorticity in Madeira's southeastern margins during the summer months. Additionally, these wind-induced eddies reached the western shores of Desertas Islands, which differed from the more static motion of the eddie found in scenario A. The latter feature, which still showed a slight southeastward motion, was potentially prevented from reaching the same destination due to the interaction with strong tidal currents in the vicinity of the Desertas ridge (Reis et al., in preparation). Such tide-related processes were prominent in the simulation results of scenario C, hence also included in scenario A, but absent in scenario B where the identified eddies would not have been interfered with (Fig. 17). Also, it is important to note the influence of the adjacent anticyclonic mesoscale eddie in this episode. Because the geostrophic currents are still being forced on this simulation, this large eddie, with high surface velocity (Fig. 17e-f), could be a factor in the formation and propagation of the submesoscale eddies. Indeed, various studies have shown that submesoscale vortices can be generated along the turbulent margins of long-lived mesoscale eddies, particularly anticyclonic ones (Capet *et al.*, 2008b; Zatsepin *et al.*, 2019; Zhong & Bracco, 2013). It could also explain the higher EKE measured within the smaller eddies (Fig. 17 g-h).

In contrast, the northern set of small-scale eddies observed in scenario B (Fig. 18) does not correlate with previously stated hypotheses. These eddies at this location might be due to the interaction of the incident far-field flows with the island shelf. However, such eddies are not found at the same moment in scenario D, where only geostrophic forces are considered. Therefore, local winds most likely interact with the incoming current to generate this set of vortices. Moreover, being the longest-lasting event found in this study and its alongshore motion, these types of submesoscale eddies have the potential to transport coastal material further along the shelf. This finding improves our knowledge on the role of nearshore submesoscale eddies in the local coastal circulation.

Meanwhile, the submesoscale eddie identified on the north coast in scenario D could be a result of the larger nearby anticyclonic eddie and its interaction with the island's sloping topography (Fig. 19). Indeed, incoming far-field mesoscale eddies, when encountering the shallow bathymetry of deep-ocean islands, can be deflected or split, the latter result being

responsible for the generation of island-transformed eddies (Cardoso *et al.*, 2020). This theory also concurs with results from Morvan *et al.* (2019), who, using numerical simulations, discovered that submesoscale eddies were induced by the interaction of mesoscale eddies and the shelf break. The authors further concluded that this phenomenon was an effective mechanism to transfer kinetic energy from the larger to the smaller scales. Furthermore, as previously mentioned, it is well known that submesoscale vortices occur on the edges of larger, quasi-geostrophic anticyclonic eddies. This could explain the formation of such a perceivable submesoscale eddie at the periphery of a mesoscale anticyclone under purely geostrophic far-field forcing conditions. Moreover, the strain-dominant area between the meso- and submesoscale eddies could have biological implications since it is commonly associated with upwelling and downwelling motions capable of transporting nutrients vertically, thus affecting phytoplankton dynamics (Xiu *et al.*, 2022).

This study was limited by the available resolution of the model at the time of computation. Overall, model outputs of 1-km resolution were sufficient for a general overview of submesoscale activity in the region. However, given the COAWST's ability to produce 300-m (and higher) resolution grids, any improvement on the resolution would have greatly enhanced the accuracy of model results at the submesoscale. Another major limitation was the lack of real observations in the spatio-temporal analysis. Complementing in-situ data with model data in the context of short-lived and small-scale eddies would have allowed for a much more complete characterization of such features. The available data for this specific monthly timeframe, however, was not adequate to be included in the study.

7. Conclusion

The objective of this study was to investigate the role of submesoscale processes in the coastal circulation of Madeira and to evaluate the ocean response to various forcing scenarios. Overall, submesoscale activity was observed mostly near coastal waters. Relative vorticity and Okubo-Weiss were the best indicators of submesoscale features, while divergence and strain were not as relevant parameters. Various episodes of submesoscale eddies with *Ro* O(1) were found on the north and southeastern coasts in scenarios A-B-D, which generally agrees with island wake and far-field current studies. These eddies were the dominant feature within Madeira's coast and were seen traveling along or sitting on the insular shelf, pointing towards a significant contribution in the coastal transport or retention of particles. Finally, wind and geostrophic currents were independently or cooperatively the most influential physical forcings in promoting submesoscale activity.

This was an exploratory study, merely opening the door to the topic of submesoscale processes in Madeira. However, these results only added a small piece to the puzzle that are the complex coastal dynamics of this deep-sea island. All in all, the study on submesoscale processes within this insular coastal area remains scarce and one to be broadened.

One way to remedy this would be to integrate Lagrangian techniques, such as drifting buoys and simulations of virtual particles, to get a better grasp of the dispersal behavior of submesoscale structures, particularly the ones discussed in the spatio-temporal analysis. In fact, the Lagrangian approach, which follows passively the motion of water parcels, is generally the preferred method to monitor submesoscale currents and their dispersion mechanisms at the ocean surface (Haza et al., 2010; Nencioli et al., 2011; Ohlmann et al., 2017; Petrenko et al., 2017). Understanding Lagrangian two-dimensional surface flows is particularly essential for tracking buoyant materials and passive tracers, such as oil spills (Poje *et al.*, 2014), marine plastic litter (Cardoso & Caldeira, 2021) and harmful algal blooms (Havens *et al.*, 2010; Olascoaga *et al.*, 2008), thus having great implications for operational oceanography and predictive modeling.

Future studies should also look at the depth signature of these types of events to obtain a broader picture of the scale at which various conditions affect submesoscale activity in the area. Additionally, information on the depth until which these features operate would

significantly improve our understanding of the vertical transport mechanisms associated with submesoscale processes and their potential interactions with the bottom boundary layer.

References

Ajayi, A., Le Sommer, J., Chassignet, E. P., Molines, J., Xu, X., Albert, A., & Dewar, W. (2021). Diagnosing Cross-Scale Kinetic Energy Exchanges From Two Submesoscale Permitting Ocean Models. *Journal of Advances in Modeling Earth Systems*, *13*(6). https://doi.org/10.1029/2019MS001923

Alpers, W., Brandt, P., Lazar, A., Dagorne, D., Sow, B., Faye, S., Hansen, M. W., Rubino, A., Poulain, P.-M., & Brehmer, P. (2013). A small-scale oceanic eddy off the coast of West Africa studied by multi-sensor satellite and surface drifter data. *Remote Sensing of Environment*, *129*, 132–143. https://doi.org/10.1016/j.rse.2012.10.032

Alves, J. M. R., Caldeira, R. M. A., & Miranda, P. M. A. (2020). Dynamics and oceanic response of the Madeira tip-jets. *Quarterly Journal of the Royal Meteorological Society*, *146*(732), 3048–3063. https://doi.org/10.1002/qj.3825

Alves, J. M. R., Tomé, R., Caldeira, R. M. A., & Miranda, P. M. A. (2021). Asymmetric Ocean Response to Atmospheric Forcing in an Island Wake: A 35-Year High-Resolution Study. *Frontiers in Marine Science*, *8*, 624392. https://doi.org/10.3389/fmars.2021.624392

Andrade, I., Sangrà, P., Hormazabal, S., & Correa-Ramirez, M. (2014). Island Mass Effect in the Juan Fernández Archipelago (33°S), Southeastern Pacific. *Deep Sea Research Part I: Oceanographic Research Papers*, *84*, 86–99. https://doi.org/10.1016/j.dsr.2013.10.009

Archer, M. R., Shay, L. K., Jaimes, B., & Martinez-Pedraja, J. (2015). Observing Frontal Instabilities of the Florida Current Using High Frequency Radar. In *Coastal Ocean Observing Systems* (pp. 179–208). Elsevier. https://doi.org/10.1016/B978-0-12-802022-7.00011-0

Azevedo, C. C., Camargo, C. M. L., Alves, J., & Caldeira, R. M. A. (2021). Convection and Heat Transfer in Island (Warm) Wakes. *Journal of Physical Oceanography*, *51*(4), 1187–1203. https://doi.org/10.1175/JPO-D-20-0103.1

Balwada, D., Smith, K. S., & Abernathey, R. (2018). Submesoscale Vertical Velocities Enhance Tracer Subduction in an Idealized Antarctic Circumpolar Current. *Geophysical Research Letters*, *45*(18), 9790–9802. https://doi.org/10.1029/2018GL079244

Becker, J. J., Sandwell, D. T., Smith, W. H. F., Braud, J., Binder, B., Depner, J., Fabre, D., Factor, J., Ingalls, S., Kim, S.-H., Ladner, R., Marks, K., Nelson, S., Pharaoh, A., Trimmer, R., Von Rosenberg, J., Wallace, G., & Weatherall, P. (2009). Global Bathymetry and Elevation Data at 30 Arc Seconds Resolution: SRTM30_PLUS. *Marine Geodesy*, *32*(4), 355–371. https://doi.org/10.1080/01490410903297766

Berti, S., Santos, F. A. D., Lacorata, G., & Vulpiani, A. (2011). Lagrangian Drifter Dispersion in the Southwestern Atlantic Ocean. *Journal of Physical Oceanography*, *41*(9), 1659–1672. https://doi.org/10.1175/2011JPO4541.1

Boccaletti, G., Ferrari, R., & Fox-Kemper, B. (2007). Mixed Layer Instabilities and Restratification. *Journal of Physical Oceanography*, *37*(9), 2228–2250. https://doi.org/10.1175/JPO3101.1

Bolado-Penagos, M., González, C. J., Chioua, J., Sala, I., Jesús Gomiz-Pascual, J., Vázquez, Á., & Bruno, M. (2020). Submesoscale Processes in the Coastal Margins of the Strait of Gibraltar. The Trafalgar – Alboran Connection. *Progress in Oceanography*, *181*, 102219. https://doi.org/10.1016/j.pocean.2019.102219

Bosse, A., Testor, P., Mayot, N., Prieur, L., D'Ortenzio, F., Mortier, L., Le Goff, H., Gourcuff, C., Coppola, L., Lavigne, H., & Raimbault, P. (2017). A Submesoscale Coherent Vortex in the Ligurian Sea: From Dynamical Barriers to Biological Implications: A Postconvective SCV in the NW Med Sea. *Journal of Geophysical Research: Oceans*, *122*(8), 6196–6217. https://doi.org/10.1002/2016JC012634

Brannigan, L., Marshall, D. P., Naveira-Garabato, A., & George Nurser, A. J. (2015). The Seasonal Cycle of Submesoscale Flows. *Ocean Modelling*, *92*, 69–84. https://doi.org/10.1016/j.ocemod.2015.05.002

Brody, S. R., Lozier, M. S., & Mahadevan, A. (2016). Quantifying the Impact of Submesoscale Processes on the Spring Phytoplankton Bloom in a Turbulent Upper Ocean Using a Lagrangian Approach. *Geophysical Research Letters*, *43*(10), 5160–5169. https://doi.org/10.1002/2016GL068051

Buckingham, C. E., Naveira Garabato, A. C., Thompson, A. F., Brannigan, L., Lazar, A., Marshall, D. P., George Nurser, A. J., Damerell, G., Heywood, K. J., & Belcher, S. E. (2016). Seasonality of Submesoscale Flows in the Ocean Surface Boundary Layer. *Geophysical Research Letters*, *43*(5), 2118–2126. https://doi.org/10.1002/2016GL068009

Caldeira, R. M. A., Groom, S., Miller, P., Pilgrim, D., & Nezlin, N. P. (2002). Sea-surface Signatures of the Island Mass Effect Phenomena Around Madeira Island, Northeast Atlantic. *Remote Sensing of Environment*, *80*(2), 336–360. https://doi.org/10.1016/S0034-4257(01)00316-9

Caldeira, R. M. A., Marchesiello, P., Nezlin, N. P., DiGiacomo, P. M., & McWilliams, J. C. (2005). Island Wakes in the Southern California Bight. *Journal of Geophysical Research*, *110*(C11), C11012. https://doi.org/10.1029/2004JC002675

Caldeira, R. M. A., & Sangrà, P. (2012). Complex Geophysical Wake Flows: Madeira Archipelago Case Study. *Ocean Dynamics*, *62*(5), 683–700. https://doi.org/10.1007/s10236-012-0528-6

Caldeira, R. M. A., Stegner, A., Couvelard, X., Araújo, I. B., Testor, P., & Lorenzo, A. (2014). Evolution of an Oceanic Anticyclone in the Lee of Madeira Island: In situ and Remote Sensing Survey. *Journal of Geophysical Research: Oceans*, *119*(2), 1195–1216. https://doi.org/10.1002/2013JC009493

Caldeira, R. M. A., & Tomé, R. (2013). Wake Response to an Ocean-Feedback Mechanism: Madeira Island Case Study. *Boundary-Layer Meteorology*, *148*(2), 419–436. https://doi.org/10.1007/s10546-013-9817-y

Callies, J., Ferrari, R., Klymak, J. M., & Gula, J. (2015). Seasonality in Submesoscale Turbulence. *Nature Communications*, *6*(1), 6862. https://doi.org/10.1038/ncomms7862

Calvert, D., Nurser, G., Bell, M. J., & Fox-Kemper, B. (2020). The Impact of a Parameterisation of Submesoscale Mixed Layer Eddies on Mixed Layer Depths in the NEMO Ocean Model. *Ocean Modelling*, *154*, 101678. https://doi.org/10.1016/j.ocemod.2020.101678

Canning-Clode, J., Kaufmann, M., Molis, M., Wahl, M., & Lenz, M. (2008). Influence of Disturbance and Nutrient Enrichment on Early Successional Fouling Communities in an Oligotrophic Marine System. *Marine Ecology*, *29*(1), 115–124. https://doi.org/10.1111/j.1439-0485.2007.00210.x

Capet, X., Campos, E. J., & Paiva, A. M. (2008). Submesoscale Activity Over the Argentinian Shelf. *Geophysical Research Letters*, *35*(15), L15605. https://doi.org/10.1029/2008GL034736

Capet, X., McWilliams, J. C., Molemaker, M. J., & Shchepetkin, A. F. (2008a). Mesoscale to Submesoscale Transition in the California Current System. Part I: Flow Structure, Eddy Flux, and Observational Tests. *Journal of Physical Oceanography*, *38*(1), 29–43. https://doi.org/10.1175/2007JPO3671.1

Capet, X., McWilliams, J. C., Molemaker, M. J., & Shchepetkin, A. F. (2008b). Mesoscale to Submesoscale Transition in the California Current System. Part II: Frontal Processes. *Journal of Physical Oceanography*, *38*(1), 44–64. https://doi.org/10.1175/2007JPO3672.1

Cardoso, C., & Caldeira, R. M. A. (2021). Modeling the Exposure of the Macaronesia Islands (NE Atlantic) to Marine Plastic Pollution. *Frontiers in Marine Science*, *8*, 653502. https://doi.org/10.3389/fmars.2021.653502

Cardoso, C., Caldeira, R. M. A., Relvas, P., & Stegner, A. (2020). Islands as Eddy Transformation and Generation Hotspots: Cabo Verde Case Study. *Progress in Oceanography*, *184*, 102271. https://doi.org/10.1016/j.pocean.2020.102271

Carlson, D. F., Muscarella, P. A., Gildor, H., Lipphardt, B. L., & Fredj, E. (2010). How Useful Are Progressive Vector Diagrams for Studying Coastal Ocean Transport? *Limnology and Oceanography: Methods*, *8*(3), 98–106. https://doi.org/10.4319/lom.2010.8.0098

Carlson, D. F., Özgökmen, T., Novelli, G., Guigand, C., Chang, H., Fox-Kemper, B., Mensa, J., Mehta, S., Fredj, E., Huntley, H., Kirwan, A. D., Berta, M., Rebozo, M., Curcic, M., Ryan, E., Lund, B., Haus, B., Molemaker, J., Hunt, C., … Horstmann, J. (2018). Surface Ocean Dispersion Observations From the Ship-Tethered Aerostat Remote Sensing System. *Frontiers in Marine Science*, *5*, 479. https://doi.org/10.3389/fmars.2018.00479

Chang, M.-H., Tang, T. Y., Ho, C.-R., & Chao, S.-Y. (2013). Kuroshio-induced Wake in the Lee of Green Island off Taiwan. *Journal of Geophysical Research: Oceans*, *118*(3), 1508–1519. https://doi.org/10.1002/jgrc.20151

Chavanne, C., Flament, P., & Gurgel, K.-W. (2010). Interactions between a Submesoscale Anticyclonic Vortex and a Front. *Journal of Physical Oceanography*, *40*(8), 1802–1818. https://doi.org/10.1175/2010JPO4055.1

Couvelard, X., Caldeira, R. M. A., Araújo, I. B., & Tomé, R. (2012). Wind Mediated Vorticity-Generation and Eddy-Confinement, Leeward of the Madeira Island: 2008 Numerical Case Study. *Dynamics of Atmospheres and Oceans*, *58*, 128–149. https://doi.org/10.1016/j.dynatmoce.2012.09.005

D'Asaro, E. A., Carlson, D. F., Chamecki, M., Harcourt, R. R., Haus, B. K., Fox-Kemper, B., Molemaker, M. J., Poje, A. C., & Yang, D. (2020). Advances in Observing and Understanding Small-Scale Open Ocean Circulation During the Gulf of Mexico Research Initiative Era. *Frontiers in Marine Science*, *7*, 349. https://doi.org/10.3389/fmars.2020.00349

D'Asaro, E. A., Lee, C., Rainville, L., Harcourt, R., & Thomas, L. (2011). Enhanced Turbulence and Energy Dissipation at Ocean Fronts. *Science*, *332*(6027), 318–322. https://doi.org/10.1126/science.1201515

D'Asaro, E. A., Shcherbina, A. Y., Klymak, J. M., Molemaker, J., Novelli, G., Guigand, C. M., Haza, A. C., Haus, B. K., Ryan, E. H., Jacobs, G. A., Huntley, H. S., Laxague, N. J. M., Chen, S., Judt, F., McWilliams, J. C., Barkan, R., Kirwan, A. D., Poje, A. C., & Özgökmen, T. M. (2018). Ocean convergence and the dispersion of flotsam. *Proceedings of the National Academy of Sciences*, *115*(6), 1162–1167. https://doi.org/10.1073/pnas.1718453115

Dauhajre, D. P., McWilliams, J. C., & Renault, L. (2019). Nearshore Lagrangian Connectivity: Submesoscale Influence and Resolution Sensitivity. *Journal of Geophysical Research: Oceans*, *124*(7), 5180–5204. https://doi.org/10.1029/2019JC014943

Dauhajre, D. P., McWilliams, J. C., & Uchiyama, Y. (2017). Submesoscale Coherent Structures on the Continental Shelf. *Journal of Physical Oceanography*, *47*(12), 2949–2976. https://doi.org/10.1175/JPO-D-16-0270.1

Delandmeter, P., Lambrechts, J., Marmorino, G. O., Legat, V., Wolanski, E., Remacle, J.-F., Chen, W., & Deleersnijder, E. (2017). Submesoscale Tidal Eddies in the Wake of Coral Islands and Reefs: Satellite Data and Numerical Modelling. *Ocean Dynamics*, *67*(7), 897–913. https://doi.org/10.1007/s10236-017-1066-z

Dong, C., Mavor, T., Nencioli, F., Jiang, S., Uchiyama, Y., McWilliams, J. C., Dickey, T., Ondrusek, M., Zhang, H., & Clark, D. K. (2009). An Oceanic Cyclonic Eddy on the Lee Side of Lanai Island, Hawai'i. *Journal of Geophysical Research*, *114*(C10), C10008. https://doi.org/10.1029/2009JC005346

Dong, C., & McWilliams, J. C. (2007). A Numerical Study of Island Wakes in the Southern California Bight. *Continental Shelf Research*, *27*(9), 1233–1248. https://doi.org/10.1016/j.csr.2007.01.016

Du, Y., Dong, X., Jiang, X., Zhang, Y., Zhu, D., Sun, Q., Wang, Z., Niu, X., Chen, W., Zhu, C., Jing, Z., Tang, S., Li, Y., Chen, J., Chu, X., Xu, C., Wang, T., He, Y., Han, B., … Peng, S. (2021). Ocean Surface Current Multiscale Observation Mission (OSCOM): Simultaneous Measurement of Ocean Surface Current, Vector Wind, and Temperature. *Progress in Oceanography*, *193*, 102531. https://doi.org/10.1016/j.pocean.2021.102531

Egbert, G. D., & Erofeeva, S. Y. (2002). Efficient Inverse Modeling of Barotropic Ocean Tides. *Journal of Atmospheric and Oceanic Technology*, *19*(2), 183–204. https://doi.org/10.1175/1520-0426(2002)019<0183:EIMOBO>2.0.CO;2

Esposito, G., Berta, M., Centurioni, L., Johnston, T. M. S., Lodise, J., Özgökmen, T., Poulain, P.-M., & Griffa, A. (2021). Submesoscale Vorticity and Divergence in the Alboran Sea: Scale and Depth Dependence. *Frontiers in Marine Science*, *8*, 678304. https://doi.org/10.3389/fmars.2021.678304

Fox-Kemper, B., & Ferrari, R. (2008). Parameterization of Mixed Layer Eddies. Part II: Prognosis and Impact. *Journal of Physical Oceanography*, *38*(6), 1166–1179. https://doi.org/10.1175/2007JPO3788.1

Giddy, I., Swart, S., du Plessis, M., Thompson, A. F., & Nicholson, S. -A. (2021). Stirring of Sea-Ice Meltwater Enhances Submesoscale Fronts in the Southern Ocean. *Journal of Geophysical Research: Oceans*, *126*(4). https://doi.org/10.1029/2020JC016814

Gildor, H., Fredj, E., Steinbuck, J., & Monismith, S. (2009). Evidence for Submesoscale Barriers to Horizontal Mixing in the Ocean from Current Measurements and Aerial Photographs. *Journal of Physical Oceanography*, *39*(8), 1975–1983. https://doi.org/10.1175/2009JPO4116.1

Gommenginger, C., Chapron, B., Hogg, A., Buckingham, C., Fox-Kemper, B., Eriksson, L., Soulat, F., Ubelmann, C., Ocampo-Torres, F., Nardelli, B. B., Griffin, D., Lopez-Dekker, P., Knudsen, P., Andersen, O., Stenseng, L., Stapleton, N., Perrie, W., Violante-Carvalho, N., Schulz-Stellenfleth, J., … Burbidge, G. (2019). SEASTAR: A Mission to Study Ocean Submesoscale Dynamics and Small-Scale Atmosphere-Ocean Processes in Coastal, Shelf and Polar Seas. *Frontiers in Marine Science*, *6*, 457. https://doi.org/10.3389/fmars.2019.00457

Gruber, N., Lachkar, Z., Frenzel, H., Marchesiello, P., Münnich, M., McWilliams, J. C., Nagai, T., & Plattner, G.-K. (2011). Eddy-induced Reduction of Biological Production in Eastern Boundary Upwelling Systems. *Nature Geoscience*, *4*(11), 787–792. https://doi.org/10.1038/ngeo1273

Gula, J., Molemaker, M. J., & McWilliams, J. C. (2014). Submesoscale Cold Filaments in the Gulf Stream. *Journal of Physical Oceanography*, *44*(10), 2617–2643. https://doi.org/10.1175/JPO-D-14-0029.1

Gula, J., Taylor, J., Shcherbina, A., & Mahadevan, A. (2021). Submesoscale Processes and Mixing. In *Ocean Mixing* (pp. 181–214). Elsevier. https://doi.org/10.1016/B978-0-12-821512-8.00015-3

Hauschildt, J., Thomsen, S., Echevin, V., Oschlies, A., José, Y. S., Krahmann, G., Bristow, L. A., & Lavik, G. (2021). The Fate of Upwelled Nitrate off Peru Shaped by Submesoscale Filaments and Fronts. *Biogeosciences*, *18*(12), 3605–3629. https://doi.org/10.5194/bg-18-3605-2021

Havens, H., Luther, M. E., Meyers, S. D., & Heil, C. A. (2010). Lagrangian Particle Tracking of a Toxic Dinoflagellate Bloom Within the Tampa Bay Estuary. *Marine Pollution Bulletin*, *60*(12), 2233–2241. https://doi.org/10.1016/j.marpolbul.2010.08.013

Haza, A. C., Özgökmen, T. M., Griffa, A., Molcard, A., Poulain, P.-M., & Peggion, G. (2010). Transport properties in small-scale coastal flows: Relative dispersion from VHF radar measurements in the

Gulf of La Spezia. *Ocean Dynamics*, *60*(4), 861–882. https://doi.org/10.1007/s10236-010-0301-7

Jaffe, J. S., Franks, P. J. S., Roberts, P. L. D., Mirza, D., Schurgers, C., Kastner, R., & Boch, A. (2017). A Swarm of Autonomous Miniature Underwater Robot Drifters for Exploring Submesoscale Ocean Dynamics. *Nature Communications*, *8*(1), 14189. https://doi.org/10.1038/ncomms14189

Jensen, T. G., Shulman, I., Wijesekera, H. W., Anderson, S., & Ladner, S. (2018). Submesoscale Features and Their Interaction With Fronts and Internal Tides in a High-Resolution Coupled Atmosphere-Ocean-Wave Model of the Bay of Bengal. *Ocean Dynamics*, *68*(3), 391–410. https://doi.org/10.1007/s10236-018-1136-x

Johnson, L., Lee, C. M., D'Asaro, E. A., Thomas, L., & Shcherbina, A. (2020). Restratification at a California Current Upwelling Front. Part I: Observations. *Journal of Physical Oceanography*, *50*(5), 1455–1472. https://doi.org/10.1175/JPO-D-19-0203.1

Johnson, L., Lee, C. M., D'Asaro, E. A., Wenegrat, J. O., & Thomas, L. N. (2020). Restratification at a California Current Upwelling Front. Part II: Dynamics. *Journal of Physical Oceanography*, *50*(5), 1473–1487. https://doi.org/10.1175/JPO-D-19-0204.1

Johnston, T. M. S., Schönau, M. C., Paluszkiewicz, T., MacKinnon, J. A., Arbic, B. K., Colin, P. L., Alford, M. H., Andres, M., Centurioni, L., Graber, H. C., Helfrich, K. R., Hormann, V., Lermusiaux, P. F. J., Musgrave, R. C., Powell, B. S., Qiu, B., Rudnick, D. L., Simmons, H. L., Laurent, L. S., … Zeiden, K. L. (2019). Flow Encountering Abrupt Topography (FLEAT). *Oceanography*, *32*(4), 10–21. https://doi.org/10.5670/oceanog.2019.407

Kessouri, F., Bianchi, D., Renault, L., McWilliams, J. C., Frenzel, H., & Deutsch, C. A. (2020). Submesoscale Currents Modulate the Seasonal Cycle of Nutrients and Productivity in the California Current System. *Global Biogeochemical Cycles*, *34*(10). https://doi.org/10.1029/2020GB006578

Klein, P., Hua, B. L., Lapeyre, G., Capet, X., Le Gentil, S., & Sasaki, H. (2008). Upper Ocean Turbulence From High-Resolution 3D Simulations. *Journal of Physical Oceanography*, *38*(8), 1748–1763. https://doi.org/10.1175/2007JPO3773.1

Klein, P., & Lapeyre, G. (2009). The Oceanic Vertical Pump Induced by Mesoscale and Submesoscale Turbulence. *Annual Review of Marine Science*, *1*(1), 351–375. https://doi.org/10.1146/annurev.marine.010908.163704

Krayushkin, E., Lavrova, O., & Strochkov, A. (2019). Application of GPS/GSM Lagrangian Mini-Drifters for Coastal Ocean Dynamics Analysis. *Russian Journal of Earth Sciences*, *19*(1), 1–16. https://doi.org/10.2205/2018ES000642

Kubryakov, A. A., Lishaev, P. N., Chepyzhenko, A. I., Aleskerova, A. A., Kubryakova, E. A., Medvedeva, A. V., & Stanichny, S. V. (2021). Impact of Submesoscale Eddies on the Transport of Suspended Matter in the Coastal Zone of Crimea Based on Drone, Satellite, and In Situ Measurement Data. *Oceanology*, *61*(2), 159–172. https://doi.org/10.1134/S0001437021020107

Lapeyre, G., Klein, P., & Hua, B. L. (2006). Oceanic Restratification Forced by Surface Frontogenesis. *Journal of Physical Oceanography*, *36*(8), 1577–1590. https://doi.org/10.1175/JPO2923.1

Lathuiliere, C., Levy, M., & Echevin, V. (2011). Impact of Eddy-driven Vertical Fluxes on Phytoplankton Abundance in the Euphotic Layer. *Journal of Plankton Research*, *33*(5), 827–831. https://doi.org/10.1093/plankt/fbq131

Lellouche, J.-M., Greiner, E., Le Galloudec, O., Régnier, C., Benkiran, M., Testut, C.-E., Bourdallé-Badie, R., Drévillon, M., Garric, G., & Drillet, Y. (2018). The Mercator Ocean Global High-Resolution Monitoring and Forecasting System. In E. P. Chassignet, A. Pascual, J. Tintoré, & J. Verron (Eds.), *New Frontiers in Operational Oceanography*. GODAE OceanView. https://doi.org/10.17125/gov2018.ch20

Lévy, M., Ferrari, R., Franks, P. J. S., Martin, A. P., & Rivière, P. (2012). Bringing Physics to Life at the Submesoscale. *Geophysical Research Letters*, *39*(14), n/a-n/a. https://doi.org/10.1029/2012GL052756

Lévy, M., Franks, P. J. S., & Smith, K. S. (2018). The Role of Submesoscale Currents in Structuring Marine Ecosystems. *Nature Communications*, *9*(1), 4758. https://doi.org/10.1038/s41467-018-07059-3

Lévy, M., Klein, P., & Treguier, A.-M. (2001). Impact of Sub-Mesoscale Physics on Production and Subduction of Phytoplankton in an Oligotrophic Regime. *Journal of Marine Research*, *59*(4), 535–565. https://doi.org/10.1357/002224001762842181

Lévy, M., Klein, P., Tréguier, A.-M., Iovino, D., Madec, G., Masson, S., & Takahashi, K. (2010). Modifications of Gyre Circulation by Sub-Mesoscale Physics. *Ocean Modelling*, *34*(1–2), 1–15. https://doi.org/10.1016/j.ocemod.2010.04.001

Lévy, M., Resplandy, L., & Lengaigne, M. (2014). Oceanic Mesoscale Turbulence Drives Large Biogeochemical Interannual Variability at Middle and High Latitudes. *Geophysical Research Letters*, *41*(7), 2467–2474. https://doi.org/10.1002/2014GL059608

Liu, X., & Levine, N. M. (2016). Enhancement of Phytoplankton Chlorophyll by Submesoscale Frontal Dynamics in the North Pacific Subtropical Gyre. *Geophysical Research Letters*, *43*(4), 1651–1659. https://doi.org/10.1002/2015GL066996

Lumpkin, R., & Elipot, S. (2017). Surface Drifter Pair Spreading in the North Atlantic. *Journal of Geophysical Research*, *115*(C12), C12017. https://doi.org/10.1029/2010JC006338

MacKinnon, J. A., Alford, M. H., Voet, G., Zeiden, K. L., Shaun Johnston, T. M., Siegelman, M., Merrifield, S., & Merrifield, M. (2019). Eddy Wake Generation From Broadband Currents Near Palau. *Journal of Geophysical Research: Oceans*, *124*(7), 4891–4903. https://doi.org/10.1029/2019JC014945

Mahadevan, A. (2006). Modeling Vertical Motion at Ocean Fronts: Are Nonhydrostatic Effects Relevant at Submesoscales? *Ocean Modelling*, *14*(3–4), 222–240. https://doi.org/10.1016/j.ocemod.2006.05.005

Mahadevan, A. (2016). The Impact of Submesoscale Physics on Primary Productivity of Plankton. *Annual Review of Marine Science*, *8*(1), 161–184. https://doi.org/10.1146/annurev-marine-010814-015912

Mahadevan, A., D'Asaro, E., Lee, C., & Perry, M. J. (2012). Eddy-Driven Stratification Initiates North Atlantic Spring Phytoplankton Blooms. *Science*, *337*(6090), 54–58. https://doi.org/10.1126/science.1218740

Mahadevan, A., Pascual, A., Rudnick, D. L., Ruiz, S., Tintoré, J., & D'Asaro, E. (2020). Coherent Pathways for Vertical Transport from the Surface Ocean to Interior. *Bulletin of the American Meteorological Society*, *101*(11), E1996–E2004. https://doi.org/10.1175/BAMS-D-19-0305.1

Mahadevan, A., & Tandon, A. (2006). An Analysis of Mechanisms for Submesoscale Vertical Motion at Ocean Fronts. *Ocean Modelling*, *14*(3–4), 241–256. https://doi.org/10.1016/j.ocemod.2006.05.006

Mantovanelli, A., Keating, S., Wyatt, L. R., Roughan, M., & Schaeffer, A. (2017). Lagrangian and Eulerian Characterization of Two Counter-Rotating Submesoscale Eddies in a Western Boundary Current. *Journal of Geophysical Research: Oceans*, *122*(6), 4902–4921. https://doi.org/10.1002/2016JC011968

Mata, J., Fonseca, P. E., Prada, S., Rodrigues, D., Martins, S., Ramalho, R., Madeira, J., Cachão, M., Silva, C. M., & Matias, M. J. (2013). O Arquipélago da Madeira. *Geologia de Portugal*, *2-Geologia Meso-cenozóica de Portugal*, 57.

McGillicuddy, D. J., Anderson, L. A., Doney, S. C., & Maltrud, M. E. (2003). Eddy-Driven Sources and Sinks of Nutrients in the Upper Ocean: Results From a 0.1° Resolution Model of the North Atlantic: Eddy-Driven Sources and Sinks of Nutrients. *Global Biogeochemical Cycles*, *17*(2), n/a-n/a. https://doi.org/10.1029/2002GB001987

Mcwilliams, J. C. (1984). The emergence of isolated coherent vortices in turbulent flow. *Journal of Fluid Mechanics*, *146*, 21–43. https://doi.org/10.1017/S0022112084001750

McWilliams, J. C. (2003). Diagnostic Force Balance and its Limits. In O. U. Velasco Fuentes, J. Sheinbaum, & J. Ochoa (Eds.), *Nonlinear Processes in Geophysical Fluid Dynamics* (pp. 287–303). Springer Netherlands. https://doi.org/10.1007/978-94-010-0074-1_17

McWilliams, J. C. (2016). Submesoscale Currents in the Ocean. *Proceedings of the Royal Society A: Mathematical, Physical and Engineering Sciences*, *472*(2189), 20160117. https://doi.org/10.1098/rspa.2016.0117

McWilliams, J. C. (2017). Submesoscale Surface Fronts and Filaments: Secondary Circulation, Buoyancy Flux, and Frontogenesis. *Journal of Fluid Mechanics*, *823*, 391–432. https://doi.org/10.1017/jfm.2017.294

McWilliams, J. C., Colas, F., & Molemaker, M. J. (2009). Cold Filamentary Intensification and Oceanic Surface Convergence Lines. *Geophysical Research Letters*, *36*(18), L18602. https://doi.org/10.1029/2009GL039402

Mensa, J. A., Garraffo, Z., Griffa, A., Özgökmen, T. M., Haza, A., & Veneziani, M. (2013). Seasonality of the Submesoscale Dynamics in the Gulf Stream Region. *Ocean Dynamics*, *63*(8), 923–941. https://doi.org/10.1007/s10236-013-0633-1

Miranda, P. M. A., Tomé, R., Frois, L., Nogueira, M., Alves, J. M. R., Prior, V., Caldeira, R., & Dutra, E. (2021). Speed-up of the Madeira tip jets in the ERA5 climate highlights the decadal variability of the Atlantic subtropics. *Quarterly Journal of the Royal Meteorological Society*, *147*(734), 679–690. https://doi.org/10.1002/qj.3940

Molemaker, M. J., McWilliams, J. C., & Yavneh, I. (2005). Baroclinic Instability and Loss of Balance. *Journal of Physical Oceanography*, *35*(9), 1505–1517. https://doi.org/10.1175/JPO2770.1

Morrow, R., Fu, L.-L., Ardhuin, F., Benkiran, M., Chapron, B., Cosme, E., d'Ovidio, F., Farrar, J. T., Gille, S. T., Lapeyre, G., Le Traon, P.-Y., Pascual, A., Ponte, A., Qiu, B., Rascle, N., Ubelmann, C., Wang, J., & Zaron, E. D. (2019). Global Observations of Fine-Scale Ocean Surface Topography With the Surface Water and Ocean Topography (SWOT) Mission. *Frontiers in Marine Science*, *6*, 232. https://doi.org/10.3389/fmars.2019.00232

Morvan, M., L'Hégaret, P., Carton, X., Gula, J., Vic, C., de Marez, C., Sokolovskiy, M., & Koshel, K. (2019). The life cycle of submesoscale eddies generated by topographic interactions. *Ocean Science*, *15*(6), 1531–1543. https://doi.org/10.5194/os-15-1531-2019

Müller, P., McWilliams, J., & Molemaker, J. (2005). *Routes to Dissipation in the Ocean: The 2D/3D Turbulence Conundrum*. Cambridge Press.

Munk, W., Armi, L., Fischer, K., & Zachariasen, F. (2000). Spirals on the Sea. *The Royal Society*, 64.

NCEP. (2000). *NCEP FNL Operational Model Global Tropospheric Analyses, continuing from July 1999*. Research Data Archive at the National Center for Atmospheric Research, Computational and Information Systems Laboratory. https://doi.org/10.5065/D6M043C6

Nencioli, F., d'Ovidio, F., Doglioli, A. M., & Petrenko, A. A. (2011). Surface Coastal Circulation Patterns by In-Situ Detection of Lagrangian Coherent Structures. *Geophysical Research Letters*, *38*(17), n/a-n/a. https://doi.org/10.1029/2011GL048815

Ohlmann, J. C., Molemaker, M. J., Baschek, B., Holt, B., Marmorino, G., & Smith, G. (2017). Drifter Observations of Submesoscale Flow Kinematics in the Coastal Ocean. *Geophysical Research Letters*, *44*(1), 330–337. https://doi.org/10.1002/2016GL071537

Ohlmann, J. C., White, P. F., Sybrandy, A. L., & Niiler, P. P. (2005). GPS–Cellular Drifter Technology for Coastal Ocean Observing Systems. *Journal of Atmospheric and Oceanic Technology*, *22*(9), 1381–1388. https://doi.org/10.1175/JTECH1786.1

Okubo, A. (1970). Horizontal dispersion of floatable particles in the vicinity of velocity singularities such as convergences. *Deep Sea Research and Oceanographic Abstracts*, *17*(3), 445–454. https://doi.org/10.1016/0011-7471(70)90059-8

Olascoaga, M. J., Beron-Vera, F. J., Brand, L. E., & Koçak, H. (2008). Tracing the Early Development of Harmful Algal Blooms on the West Florida Shelf With the AId of Lagrangian Coherent Structures: Tracing the Early Development of HABs. *Journal of Geophysical Research: Oceans*, *113*(C12). https://doi.org/10.1029/2007JC004533

Oschlies, A. (2002). Can Eddies Make Ocean Deserts Bloom? *Global Biogeochemical Cycles*, *16*(4), 53-1-53–11. https://doi.org/10.1029/2001GB001830

Petrenko, A. A., Doglioli, A. M., Nencioli, F., Kersalé, M., Hu, Z., & d'Ovidio, F. (2017). A Review of the LATEX Project: Mesoscale to Submesoscale Processes in a Coastal Environment. *Ocean Dynamics*, *67*(3–4), 513–533. https://doi.org/10.1007/s10236-017-1040-9

Poje, A. C., Ozgokmen, T. M., Lipphardt, B. L., Haus, B. K., Ryan, E. H., Haza, A. C., Jacobs, G. A., Reniers, A. J. H. M., Olascoaga, M. J., Novelli, G., Griffa, A., Beron-Vera, F. J., Chen, S. S., Coelho, E., Hogan, P. J., Kirwan, A. D., Huntley, H. S., & Mariano, A. J. (2014). Submesoscale Dispersion in the Vicinity of the Deepwater Horizon spill. *Proceedings of the National Academy of Sciences*, *111*(35), 12693–12698. https://doi.org/10.1073/pnas.1402452111

Pullen, J., Allard, R., Seo, H., Miller, A. J., Chen, S., Pezzi, L. P., Smith, T., Chu, P., Alves, J., & Caldeira, R. (2017). Coupled ocean-atmosphere forecasting at short and medium time scales. *Journal of Marine Research*, *75*(6), 877–921. https://doi.org/10.1357/002224017823523991

Rascle, N., Chapron, B., Molemaker, J., Nouguier, F., Ocampo-Torres, F. J., Osuna Cañedo, J. P., Marié, L., Lund, B., & Horstmann, J. (2020). Monitoring Intense Oceanic Fronts Using Sea Surface Roughness: Satellite, Airplane, and In Situ Comparison. *Journal of Geophysical Research: Oceans*, *125*(8). https://doi.org/10.1029/2019JC015704

Rascle, N., Molemaker, J., Marié, L., Nouguier, F., Chapron, B., Lund, B., & Mouche, A. (2017). Intense Deformation Field at Oceanic Front Inferred From Directional Sea Surface Roughness Observations: Directional Roughness at Oceanic Front. *Geophysical Research Letters*, *44*(11), 5599–5608. https://doi.org/10.1002/2017GL073473

Romero, L., Uchiyama, Y., Ohlmann, J. C., McWilliams, J. C., & Siegel, D. A. (2013). Simulations of Nearshore Particle-Pair Dispersion in Southern California. *Journal of Physical Oceanography*, *43*(9), 1862–1879. https://doi.org/10.1175/JPO-D-13-011.1

Ruiz, S., Claret, M., Pascual, A., Olita, A., Troupin, C., Capet, A., Tovar-Sánchez, A., Allen, J., Poulain, P., Tintoré, J., & Mahadevan, A. (2019). Effects of Oceanic Mesoscale and Submesoscale Frontal Processes on the Vertical Transport of Phytoplankton. *Journal of Geophysical Research: Oceans*, *124*(8), 5999–6014. https://doi.org/10.1029/2019JC015034

Sasaki, H., Klein, P., Qiu, B., & Sasai, Y. (2014). Impact of Oceanic-Scale Interactions on the Seasonal Modulation of Ocean Dynamics by the Atmosphere. *Nature Communications*, *5*(1), 5636. https://doi.org/10.1038/ncomms6636

Schaeffer, A., Gramoulle, A., Roughan, M., & Mantovanelli, A. (2017). Characterizing Frontal Eddies Along the East Australian Current From HF Radar Observations. *Journal of Geophysical Research: Oceans*, *122*(5), 3964–3980. https://doi.org/10.1002/2016JC012171

Schubert, R., Gula, J., & Biastoch, A. (2021). Submesoscale Flows Impact Agulhas Leakage in Ocean Simulations. *Communications Earth & Environment*, *2*(1), 197. https://doi.org/10.1038/s43247-021-00271-y

Shchepetkin, A. F., & McWilliams, J. C. (2005). The Regional Oceanic Modeling System (ROMS): A Split-Explicit, Free-Surface, Topography-Following-Coordinate Oceanic Model. *Ocean Modelling*, *9*(4), 347–404. https://doi.org/10.1016/j.ocemod.2004.08.002

Shcherbina, A. Y., Sundermeyer, M. A., Kunze, E., D'Asaro, E., Badin, G., Birch, D., Brunner-Suzuki, A.-M. E. G., Callies, J., Kuebel Cervantes, B. T., Claret, M., Concannon, B., Early, J., Ferrari, R., Goodman, L., Harcourt, R. R., Klymak, J. M., Lee, C. M., Lelong, M.-P., Levine, M. D., … Ledwell, J. R. (2015). The LatMix Summer Campaign: Submesoscale Stirring in the Upper Ocean. *Bulletin of the American Meteorological Society*, *96*(8), 1257–1279. https://doi.org/10.1175/BAMS-D-14-00015.1

Shulman, I., Penta, B., Richman, J., Jacobs, G., Anderson, S., & Sakalaukus, P. (2015). Impact of Submesoscale Processes on Dynamics of Phytoplankton Filaments. *Journal of Geophysical Research: Oceans*, *120*(3), 2050–2062. https://doi.org/10.1002/2014JC010326

Siegelman, L., Klein, P., Rivière, P., Thompson, A. F., Torres, H. S., Flexas, M., & Menemenlis, D. (2020). Enhanced Upward Heat Transport at Deep Submesoscale Ocean Fronts. *Nature Geoscience*, *13*(1), 50–55. https://doi.org/10.1038/s41561-019-0489-1

Skamarock, W. C., Klemp, J. B., Dudhia, J., Gill, D. O., Barker, D. M., Duda, M. G., Huang, X.-Y., Wang, W., & Powers, J. G. (2008). A Description of the Advanced Research WRF Version 3. *NCAR Technical Notes*, *673*, 125. http://dx.doi.org/10.5065/D68S4MVH

Stammer, D. (1997). Global Characteristics of Ocean Variability Estimated From Regional TOPEX/POSEIDON Altimeter Measurements. *Journal of Physical Oceanography*, *27*(8), 1743–1769. https://doi.org/10.1175/1520-0485(1997)027<1743:GCOOVE>2.0.CO;2

Su, Z., Torres, H., Klein, P., Thompson, A. F., Siegelman, L., Wang, J., Menemenlis, D., & Hill, C. (2020). High-Frequency Submesoscale Motions Enhance the Upward Vertical Heat Transport in the Global Ocean. *Journal of Geophysical Research: Oceans*, *125*(9). https://doi.org/10.1029/2020JC016544

Su, Z., Wang, J., Klein, P., Thompson, A. F., & Menemenlis, D. (2018). Ocean Submesoscales as a Key Component of the Global Heat Budget. *Nature Communications*, *9*(1), 775. https://doi.org/10.1038/s41467-018-02983-w

Thomas, L. N., Tandon, A., & Mahadevan, A. (2008). Submesoscale Processes and Dynamics. In M. W. Hecht & H. Hasumi (Eds.), *Geophysical Monograph Series* (Vol. 177, pp. 17–38). American Geophysical Union. https://doi.org/10.1029/177GM04

Thompson, A. F., Lazar, A., Buckingham, C., Garabato, A. C. N., Damerell, G. M., & Heywood, K. J. (2016). Open-Ocean Submesoscale Motions: A Full Seasonal Cycle of Mixed Layer Instabilities from Gliders. *Journal of Physical Oceanography*, *46*, 23.

Thyng, K., Hetland, R., Filipe, & Xomchuk, V. R. (2022). *xoceanmodel/xroms: V0.1*. Zenodo. https://doi.org/10.5281/zenodo.6885972

Uchida, T., Balwada, D., P. Abernathey, R., A. McKinley, G., K. Smith, S., & Lévy, M. (2020). Vertical Eddy Iron Fluxes Support Primary Production in the Open Southern Ocean. *Nature Communications*, *11*(1), 1125. https://doi.org/10.1038/s41467-020-14955-0

Uchiyama, Y., Idica, E. Y., McWilliams, J. C., & Stolzenbach, K. D. (2014). Wastewater Effluent Dispersal in Southern California Bays. *Continental Shelf Research*, *76*, 36–52. https://doi.org/10.1016/j.csr.2014.01.002

Van Rossum, G. (2009). *Python Programming Language* (3.9). Python Software Foundation.

Warner, J. C., Armstrong, B., He, R., & Zambon, J. B. (2010). Development of a Coupled Ocean–Atmosphere–Wave–Sediment Transport (COAWST) Modeling System. *Ocean Modelling*, *35*(3), 230–244. https://doi.org/10.1016/j.ocemod.2010.07.010

Weiss, J. (1991). The dynamics of enstrophy transfer in two-dimensional hydrodynamics. *Physica D: Nonlinear Phenomena*, *48*(2–3), 273–294. https://doi.org/10.1016/0167-2789(91)90088-Q

Wijesekera, H. W., Shroyer, E., Tandon, A., Ravichandran, M., Sengupta, D., Jinadasa, S. U. P., Fernando, H. J. S., Agrawal, N., Arulananthan, K., Bhat, G. S., Baumgartner, M., Buckley, J., Centurioni, L., Conry, P., Farrar, J. T., Gordon, A. L., Hormann, V., Jarosz, E., Jensen, T. G., … Whalen, C. B. (2016). ASIRI: An Ocean–Atmosphere Initiative for Bay of Bengal. *Bulletin of the American Meteorological Society*, *97*(10), 1859–1884. https://doi.org/10.1175/BAMS-D-14-00197.1

Williams, R. G., & Follows, M. J. (2003). Physical Transport of Nutrients and the Maintenance of Biological Production. In M. J. R. Fasham (Ed.), *Ocean Biogeochemistry* (pp. 19–51). Springer Berlin Heidelberg. https://doi.org/10.1007/978-3-642-55844-3_3

Won, S. I., Kim, S. Y., & Kim, K. O. (2019). Submesoscale Surface Tidal, Vortical, and Residual Circulations in a Semienclosed Bay. *Journal of Geophysical Research: Oceans*, *124*(7), 5105–5137. https://doi.org/10.1029/2018JC014892

Wunsch, C. (2004). Vertical Mixing, Energy, and the General Circulation of the Oceans. *Annual Review of Fluid Mechanics*, *36*(1), 281–314. https://doi.org/10.1146/annurev.fluid.36.050802.122121

Xiu, P., Guo, L., & Ma, W. (2022). Modelling the influence of submesoscale processes on phytoplankton dynamics in the northern South China Sea. *Frontiers in Marine Science*, *9*, 967678. https://doi.org/10.3389/fmars.2022.967678

Yu, X., Garabato, A. C. N., Martin, A. P., Buckingham, C. E., Brannigan, L., & Su, Z. (2019). An Annual Cycle of Submesoscale Vertical Flow and Restratification in the Upper Ocean. *Journal of Physical Oceanography*, *49*, 23.

Zatsepin, A., Kubryakov, A., Aleskerova, A., Elkin, D., & Kukleva, O. (2019). Physical mechanisms of submesoscale eddies generation: Evidences from laboratory modeling and satellite data in the Black Sea. *Ocean Dynamics*, *69*(2), 253–266. https://doi.org/10.1007/s10236-018-1239-4

Zeiden, K. L., MacKinnon, J. A., Alford, M. H., Rudnick, D. L., Voet, G., & Wijesekera, H. (2021). Broadband Submesoscale Vorticity Generated by Flow around an Island. *Journal of Physical Oceanography*, *51*(4), 1301–1317. https://doi.org/10.1175/JPO-D-20-0161.1

Zhong, Y., & Bracco, A. (2013). Submesoscale Impacts on Horizontal and Vertical Transport in the Gulf of Mexico. *Journal of Geophysical Research: Oceans*, *118*(10), 5651–5668. https://doi.org/10.1002/jgrc.20402

Zhong, Y., Bracco, A., Tian, J., Dong, J., Zhao, W., & Zhang, Z. (2017). Observed and Simulated Submesoscale Vertical Pump of an Anticyclonic Eddy in the South China Sea. *Scientific Reports*, *7*(1), 44011. https://doi.org/10.1038/srep44011